SLURRY PHASE IRON CATALYSTS FOR INDIRECT COAL LIQUEFACTION

Contract No. DE-FG22-95PC95210--05

to

The University of New Mexico

7/5/94 - 7/4/98

Fifth Semi-Annual Progress Report

Covering the Period from 7/5/97 - 1/4/98

Prepared for

U.S. Department of Energy
Federal Energy Technology Center
FETC Project Manager: Richard E. Tischer

Submitted by

Abhaya K. Datye, Professor
Department of Chemical & Nuclear Engineering and
Director, Center for Micro-Engineered Materials
University of New Mexico
Albuquerque, NM 87131
submitted September 10, 1998

Disclaimer

This report was prepared as an account of work sponsored by an agency of the United States Government. Neither the United States Government nor any agency thereof, nor any of their employees, makes any warranty, express or implied, or assumes any legal liability or responsibility for the accuracy, completeness, or usefulness of any information, apparatus, product, or process disclosed, or represents that its use would not infringe privately owned rights. Reference herein to any specific commercial product, process, or service by trade name, trademark, manufacturer, or otherwise does not necessarily constitute or imply its endorsement, recommendation, or favoring by the United States Government or any agency thereof. The views and opinions of authors expressed herein do not necessarily state or reflect those of the United States Government or any agency thereof.

Disclaimer

This report was prepared as an account of work sponsored by an agency of the United States Government. Neither the United States Government nor any agency thereof, nor any of their employees, makes any warranty, express or implied, or assumes any legal liability or responsibility for the accuracy, completeness, or usefulness of any information, apparatus, product or process disclosed, or represents that its use would not infringe privately owned rights. Reference herein to any specific commercial product, or service, by trade name, trademark, manufacturer, or otherwise, does not necessarily constitute or imply its endorsement, recommendation, or favoring by the United States Government or any agency thereof. The views and opinions of authors expressed herein do not necessarily state or reflect those of the United States Government or any agency thereof.

Abstract

This report describes research conducted to support the DOE program in indirect coal liquefaction. Specifically, we have studied the attrition behavior of Iron Fischer-Tropsch catalysts, their interaction with the silica binder and the evolution of iron phases in a synthesis gas conversion process. The results provide significant insight into factors that should be considered in the design of catalysts for the conversion of coal-derived synthesis gas into liquid fuels.

Table of Contents page

Executive Summary

This report covers the fifth six-month period of this three-year grant, under the University Coal Research program. During this period, we have continued the synthesis and analysis of precipitated catalysts, using a bench-top spray dryer. We have also continued studies of the influence of binders on particle strength for doubly promoted iron catalysts on alumina, synthesized by Mr. Robert Gormley, at FETC, and compared those to catalysts synthesized here at the University of New Mexico (UNM) from doubly-promoted hematite with binders, and with a catalyst prepared by a collaborator, Mr. Ralph Brooks, Yale University, using precipitated magnetite with binders. Two methods of deriving catalyst particle breaking stress, ultrasonic fragmentation and uniaxial compaction, were applied to the catalysts, and those results will be discussed briefly. In the next six-month period, the catalysts will be analyzed by TPR in order to determine their ease of reducibility, then tested under typical FTS run conditions, to determine their relative activities and stabilities.

We have completed the preliminary X-ray diffraction analyses and data interpretation for the catalyst samples received from Fischer-Tropsch stirred-tank reactor runs being conducted at Texas A&M University (TAMU). Some of the slurry samples were sealed in epoxy and microtomed for examination by high resolution transmission electron microscopy (HRTEM). The corresponding soxhlet-extracted samples were also analyzed by HRTEM. All of the analyses, results and discussion are attached in the form of paper submitted for publication in the Fall, 1998, special issue of the Journal of Applied Catalysis. In the paper, we show that some of the problems associated with sample analysis of the working F-T catalyst originate with the difficulty in preserving the microstructures and composition intact, as the sample is prepared for analysis. We first discuss how the relative X-ray scattering cross-section differences between Fe, C, and O, can present a deceptive picture of the phase compositions in a working catalyst. We present additional evidence that Soxhlet extraction of a slurry, to obtain a relatively wax-free powder, can cause significant changes in catalyst phase composition. We have made some preliminary quantifications of the phases present in each sample, and related that information to the activity of the catalyst over the course of the run, as a function of time on-stream. We conclude that, in its most active form, the Fe catalyst in a slurry reactor consists of ϵ'-carbide (Fe_7C_3) and alpha-iron (α-Fe), while the χ-carbide which is also present, appears to be less active.

In the coming six-month period, the interpretation of the results presented in the paper will be completed. Additional Neutron diffraction studies of the catalysts will be attempted for comparison to XRD results. The influence of temperature and pressure upon the phase compositions and morphological changes observed by XRD and by Neutron Diffraction in the working catalyst in wax will be explored further, by theoretical modeling as well as experiment, and related to the data from the TAMU samples. The microtomy and analysis of more of the TAMU slurry samples by HRTEM will be completed and discussed in detail.

Technical Objectives

The objective of this research project is to perform fundamental research in support of catalyst development for slurry-phase bubble column reactors for Fischer-Tropsch synthesis. The overall program is divided into several tasks:

Task 1: **Catalyst Particulate Synthesis**. We will first study various factors which determine the attrition resistance of iron catalysts used for slurry-phase Fischer-Tropsch synthesis. The fundamental

insights gained from study of the attrition phenomenon will be used to tailor the preparation of novel precipitated catalysts. In order to determine optimal treatment protocols for these catalysts, it will be necessary to conduct investigations of catalyst microstructure, as a function of treatment method.

Task 2: **Catalyst-Binder Interactions**. Because the use of binders is considered necessary for synthesis of a catalyst with good attrition resistance, we will perform fundamental studies of catalyst binder interactions. Model catalysts will be studied, ex-situ and in-situ, by high-resolution transmission electron microscopy (HRTEM), in order to determine the nature of interfacial phases at the iron-binder interface. A better understanding of the underlying thermodynamics influencing the catalyst-binder interactions will help provide improved catalyst design criteria.

Task 3: **Characterization of used catalysts from reactors operated under typical industrial conditions**. Task 3 was not a part of the original proposal. However, we felt that, in order to design a catalyst with improved attrition resistance and high activity, a better understanding of the phenomena affecting a working catalyst's reactivity, life and stability over the course of a reaction run was needed. Consequently, samples from stirred-tank reactors operated at typical industrial FTS conditions, provided by CAER, University of Kentucky and Texas A&M University will be analyzed by X-ray diffraction, neutron diffraction, and HRTEM. The data will help us understand the causes and effects of phase compositions and morphological changes on the catalyst activity under realistic reactor conditions.

Technical Progress

Task 1 - Catalyst Particulate Synthesis

Overview

In the previous semi-annual report, we examined the particle strengths of several catalyst formulations, prepared by Mr. Robert Gormley, Federal Energy Technology Center (FETC), and brought on line a bench-top spray dryer, which is being used to make various catalysts, with and without binder. We have continued our catalyst preparation studies and evaluation of various attrition testing methods. The strengths of the spray-dried catalyst, prepared and treated by various methods, have been investigated by ultrasonic fragmentation and uniaxial compaction. Our results indicate that the method of catalyst preparation, as well as the environment to which the powders are subjected can have a significant effect on catalyst strength.

Ultrasonic Fragmentation Tests

Several catalysts, prepared by Mr. Robert Gormley, of FETC, have been analyzed for agglomerate strength by ultrasonic fragmentation. Experimental details for the ultrasonic fragmentation testing method have been described in detail in our previous reports. One gram of catalyst is dispersed in 50 ml of deionized water. A Sedigraph particle size analyzer is used to determine the particle size distribution of the suspension. The suspension is ultrasonicated, using a Tekmar high-intensity probe. After ultrasonication for varying periods of time, the suspension is reanalyzed by Sedigraph, in order to determine the mode of particle fragmentation. The results are also used to derive a quantitative measure of agglomerate strength, as explained previously in our progress reports.

Figures 1 and 2 show fragmentation results from two samples of the FETC catalyst, prepared from Fe_2O_3 promoted with K and Cu and deposited in different ways onto preformed alumina granules. These samples are

designated as AQFE/CU/K/AL-ED1-24 and AQFE/CU/K/AL-FH1-137, respectively. The first catalyst sample, -ED1-24 (figure 1), appears to be much stronger than sample -FH1-137 (figure 2), but is comparable to the Vista alumina powder discussed in the August, 1997, semi-annual report. We attribute these results to differences in treatment conditions. Figures 3 and 4 show fragmentation results from two samples of precipitated, Cu-promoted Fe catalyst, calcined at 350°C in air, prepared under different conditions. These are designated as PRFECUAL/4K-ED10-58 and as PRFECUAL/4K-ED11-117, respectively. The results show that -ED10-58 (figure 3), appears to be much stronger than -ED11-117 (figure 4), but is comparable to the Vista alumina powder discussed in the August, 1997, semi-annual report. It was stated in the August, 1997, report that calcination did not appear to significantly improve the strength of the agglomerates; therefore these results may also be attributed to differences in treatment conditions.

Next, spray-dried catalysts were prepared at UNM from Fe_2O_3 precursor with varying amounts of binder, using a Bucchi mini spray dryer. These samples were compared to similar ones using a Fe_3O_4 precursor, prepared by Mr. Ralph Brooks, Yale University. The Fe_3O_4 catalyst was synthesized as follows: A slurry of 6.5 ml, 5 weight % silica (PSA), 106 ml, 5 weight % silica (deionized Ludox SM-30), and 50 g magnetite (Fe_3O_4), was spray-dried, using a Yamato DL-41 spray dryer under the following drying conditions: atomizing air at 3 kgf/cm^2, aspirator at 0.8 m^3/min, pump at 3.5 (approximately 30 cm^3/min), drying chamber temperature of 240°C, and collecting chamber temperature of 95°C.

Figure 5 shows fragmentation results for the Fe_3O_4 catalyst. As expected, particle fragmentation is comparable to that observed in our spray-dried catalysts, as shown in the February, 1997, report. However, the Fe_3O_4 catalyst may not be active for FTS (Huang, et al., 1993). Hence, the known catalytic activity of the precursor could be an important issue to consider when preparing catalysts; therefore the activity of these two precipitated catalysts will be explored in the near future.

Uniaxial Compression Testing

The catalysts tested in the previous section were also examined using an Instron 5565 uniaxial compaction test apparatus. Experimental details, as well as a detailed discussion of the uniaxial compression method, have been described in our previous reports. Figures 6 and 7 show compaction data for the FETC catalyst shown in Figure 2, and for the Fe_3O_4 catalyst, respectively. The data are presented as a plot of ln (P) vs. natural strain, e. The results were analyzed using a model presented by Adams, et. al., 1994, which yields a value for the breaking strength, sigma (in Mpa), of the particles within the powder sample. According to these data, the catalyst prepared by depositing doubly-promoted Fe_2O_3 on preformed alumina granules is much stronger than the spray-dried Fe_3O_4 catalyst. In contrast, the ultrasonic fragmentation results imply that the spray-dried Fe_3O_4 catalyst is stronger than the doubly-promoted Fe_2O_3 on alumina. We concluded that the catalyst powder strength is affected by its environment, as well as treatment conditions.

Future Work

The effects of catalyst environment in the fluid suspension will continue to be investigated. The behavior of the two types of precipitated, spray-dried catalysts, using Fe_2O_3 and Fe_3O_4 precursors, in a model reactor, operated at typical industrial conditions will be explored. We hope to determine conclusively which of the two particle strength testing methods more accurately predicts catalyst behavior in a slurry-bubble column. Our work over the next six months will continue to explore the effectiveness and performance of the spray-dried precipitated catalysts and the effect of metal-support interactions on the attrition resistance of these catalysts.

ask 2 - Catalyst Binder Interactions
Task 3 - Characterization of used catalysts from reactors operated under typical industrial conditions

Tasks 2 and 3 are addressed together, for the purposes of this report. The progress on these two tasks is summarized in the draft publication, included as attachment A, submitted for publication in the Journal of Applied Catalysis, special issue on Fischer-Tropsch catalysis, edited by Prof. Hans Schulz.

Acknowledgments

The following graduate students participated in this project: Linda Mansker, x-ray and neutron diffraction (ND) studies; Yaming Jin, HRTEM; Hien Pham - attrition resistance studies. Undergraduate student Ralph Brooks who participated in this project over the summer of 1995 continued his studies in the form of a mini-thesis at Yale, where he graduated with a BS in Chemical Engineering in Spring 97. The HRTEM and XRD measurements were performed using the analytical facilities provided by the Earth and Planetary Sciences Department. The ND studies were performed at Los Alamos National Laboratory; Los Alamos, NM.

References

Huang, C.S.; Xu, L.; Davis, B.H.; Fuel Science and Technology, International. **11**; 639 (1993).
Adams, M. J. ; Mullier, M. A. ; and Seville, . P. K.; Powder Technology, **78**, 5 (1994).

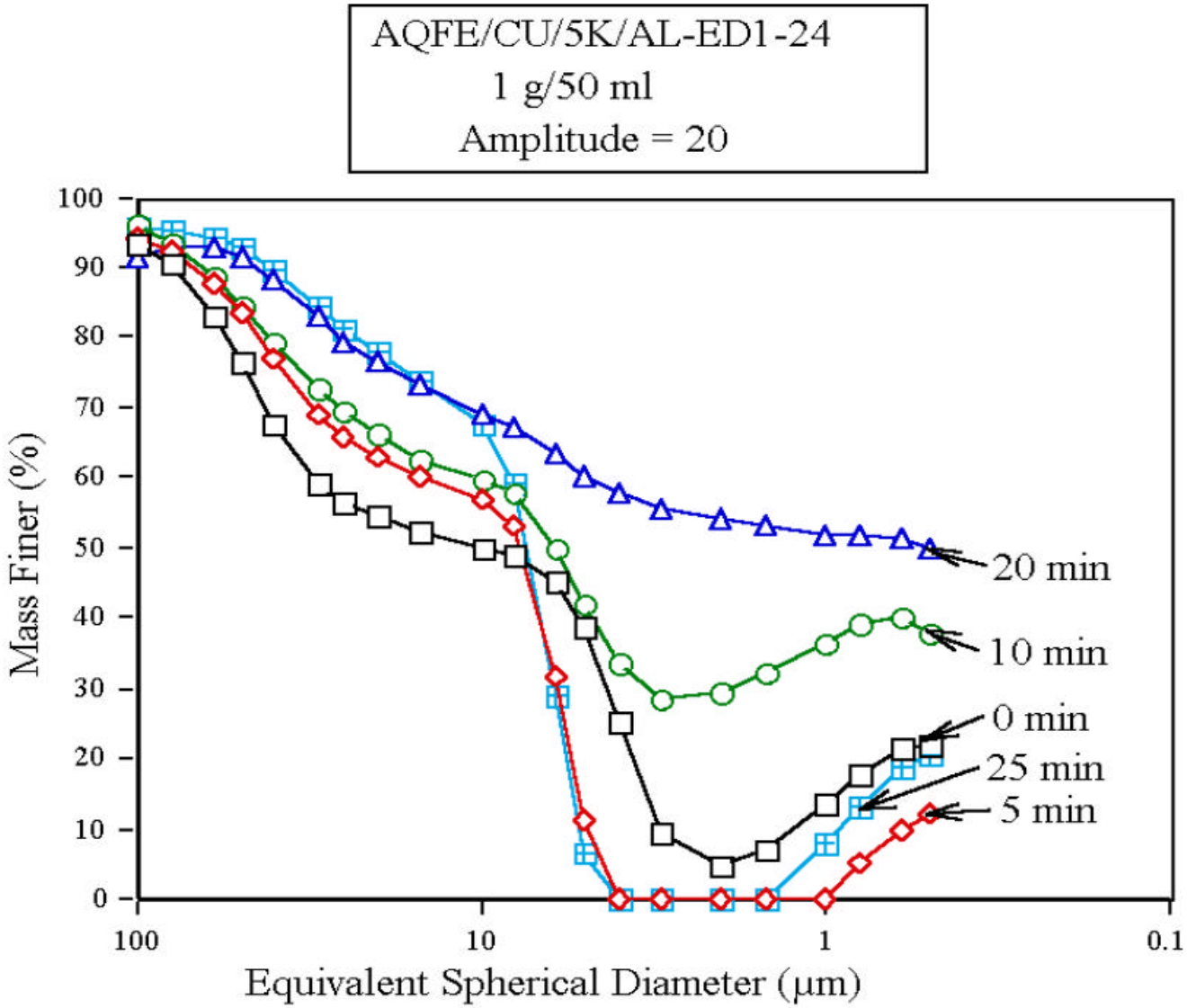

Figure 1 Ultrasonication results for a doubly-promoted iron catalyst, deposited on preformed alumina

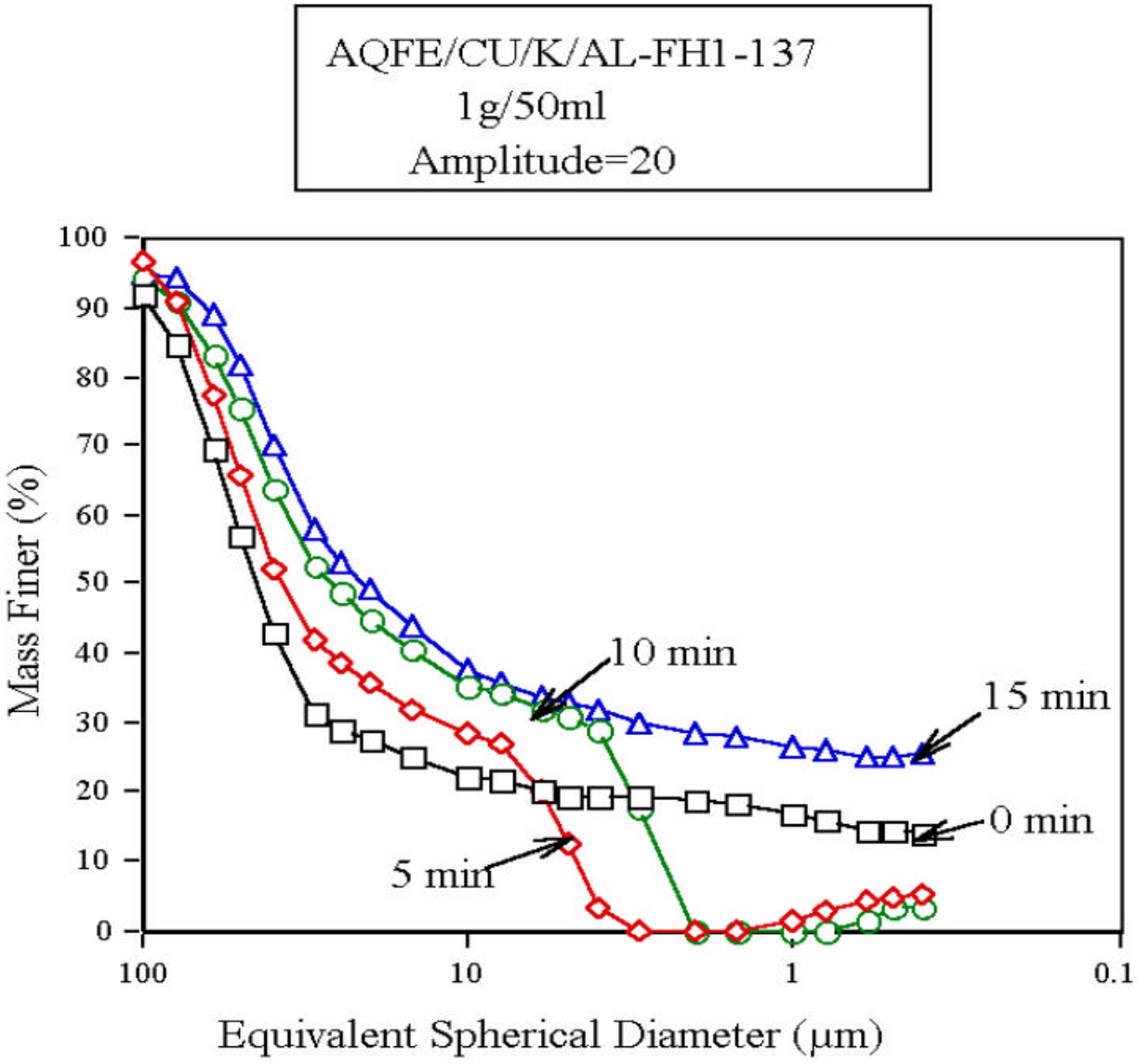

Figure 2 Ultrasonication results for a doubly-promoted iron catalyst, deposited on preformed alumina

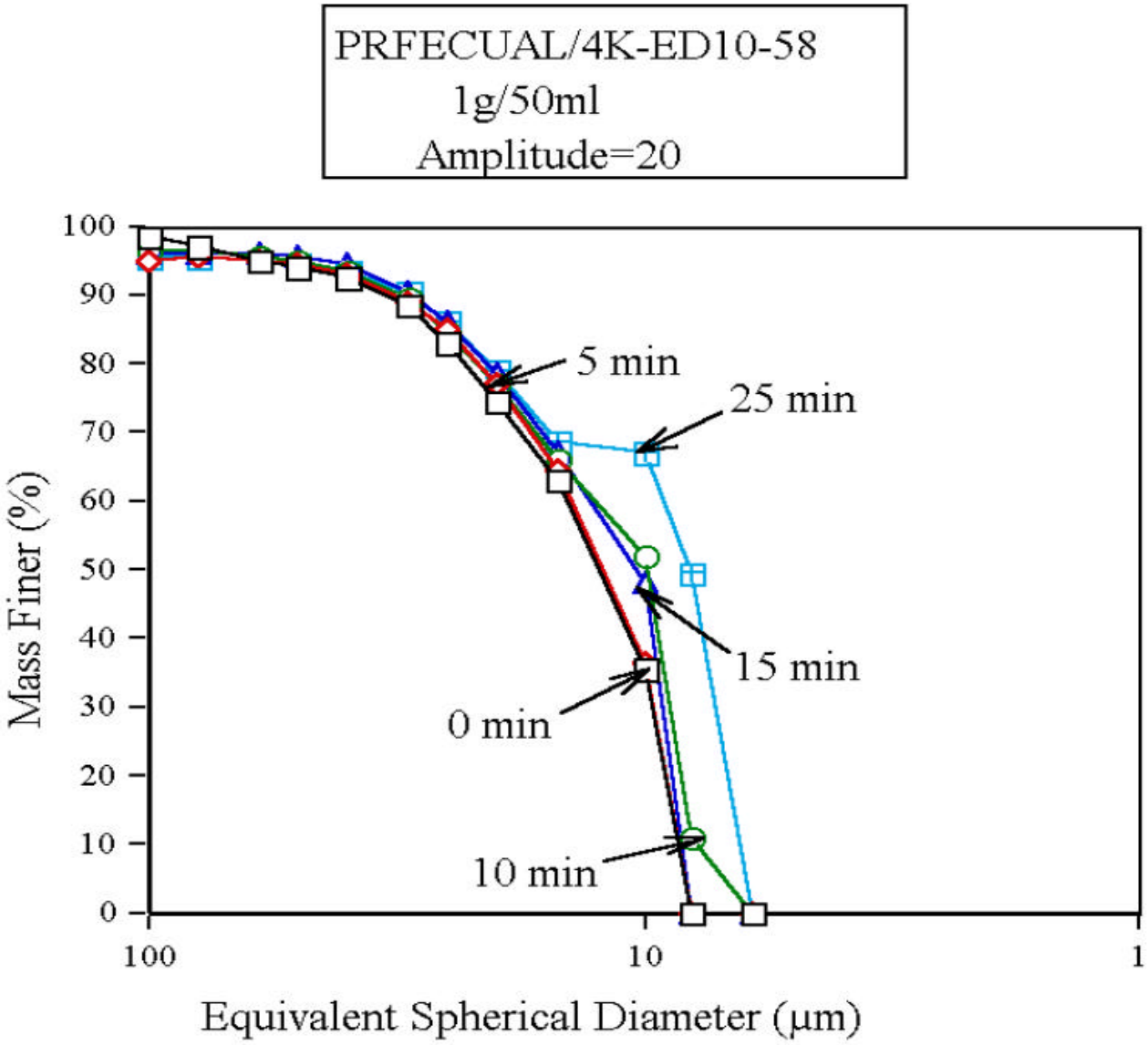

Figure 3 Ultrasonication results for a Cu-promoted iron catalyst on alumina

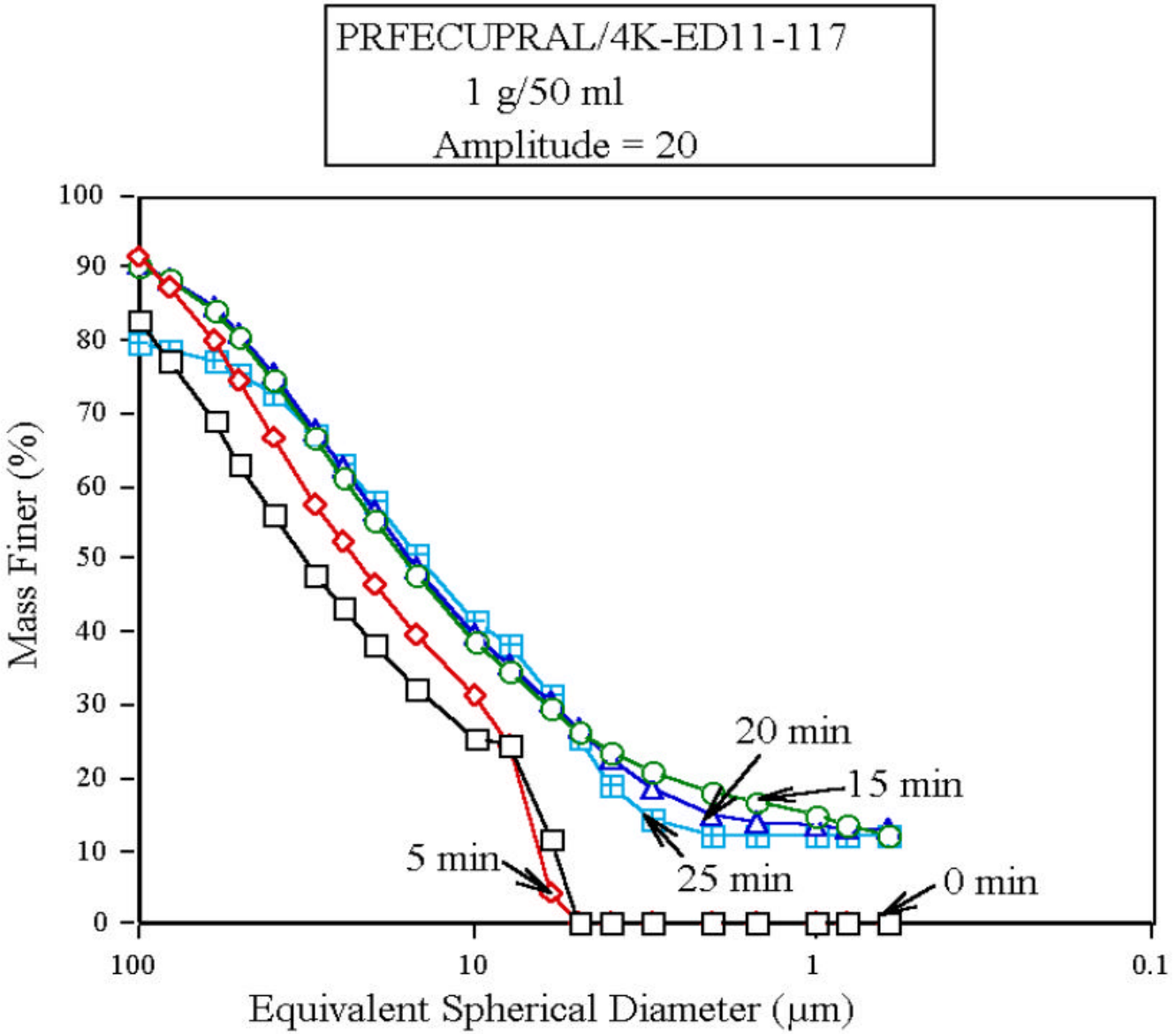

Figure 4 Ultrasonication results for a Cu-promoted iron catalyst on alumina

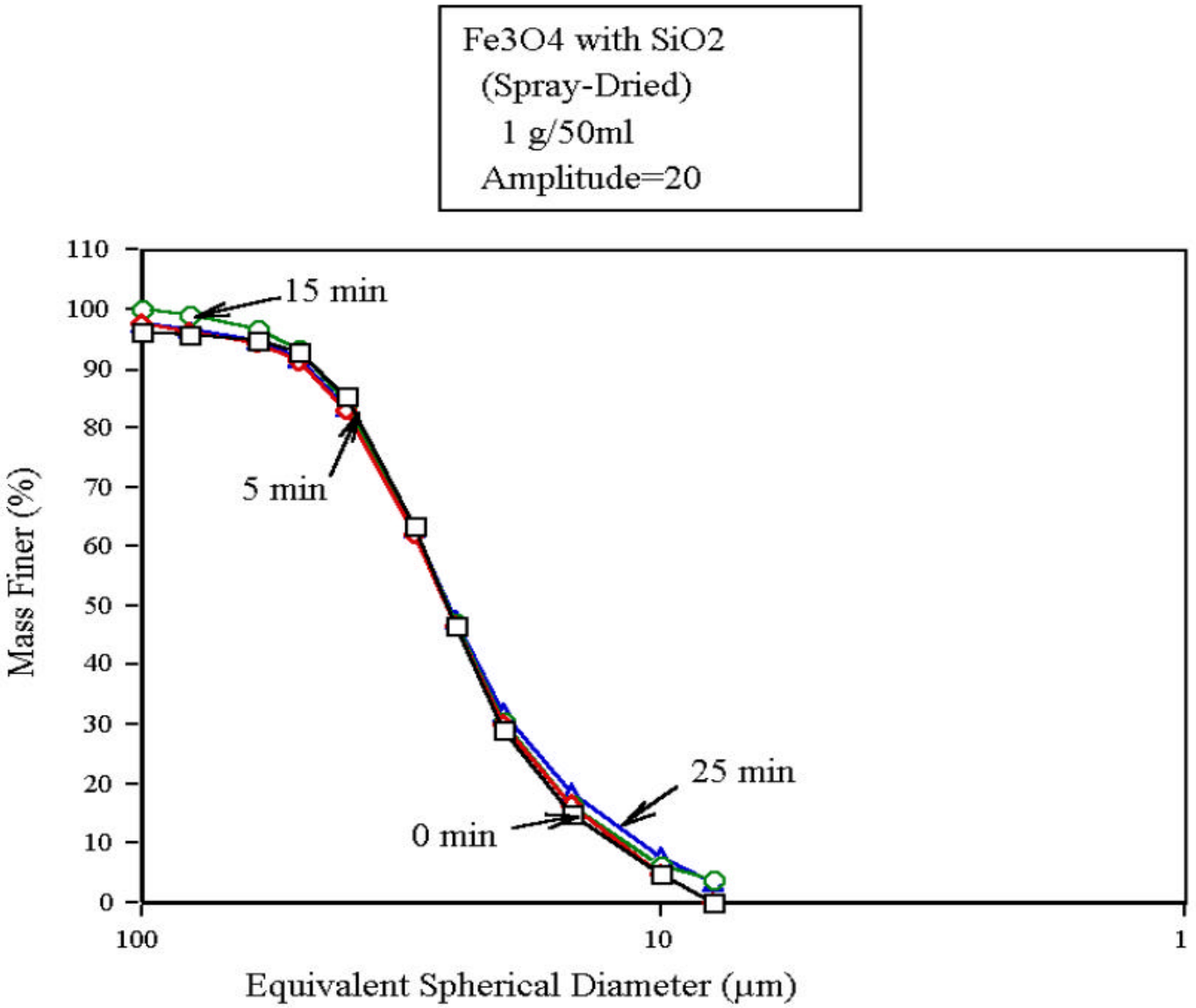

Figure 5 Ultrasonic Fragmentation Results for a spray-dried, Fe_3O_4/silica catalyst

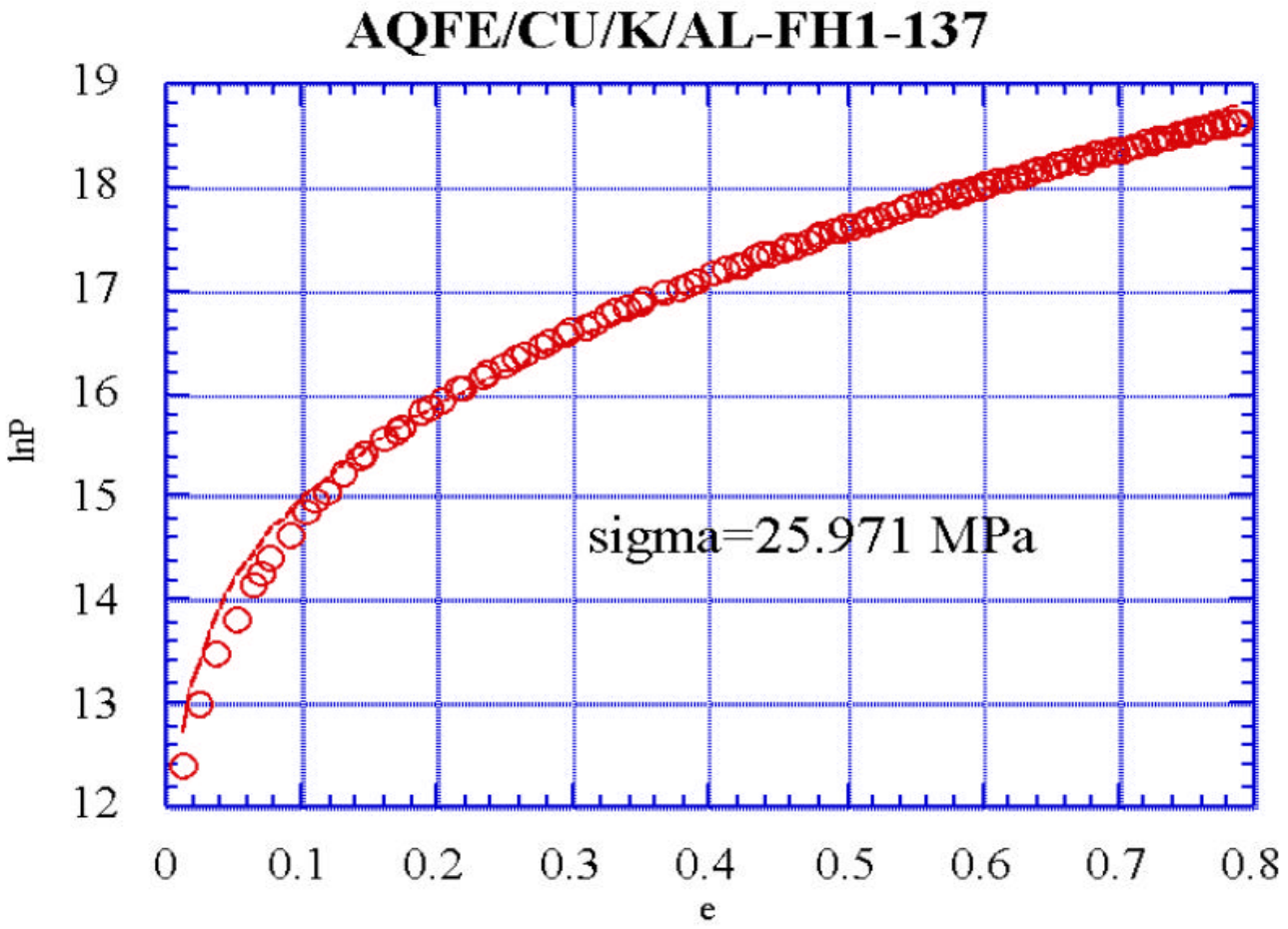

Figure 6 Uniaxial Compaction results for a doubly - promoted iron catalyst, deposited on preformed alumina

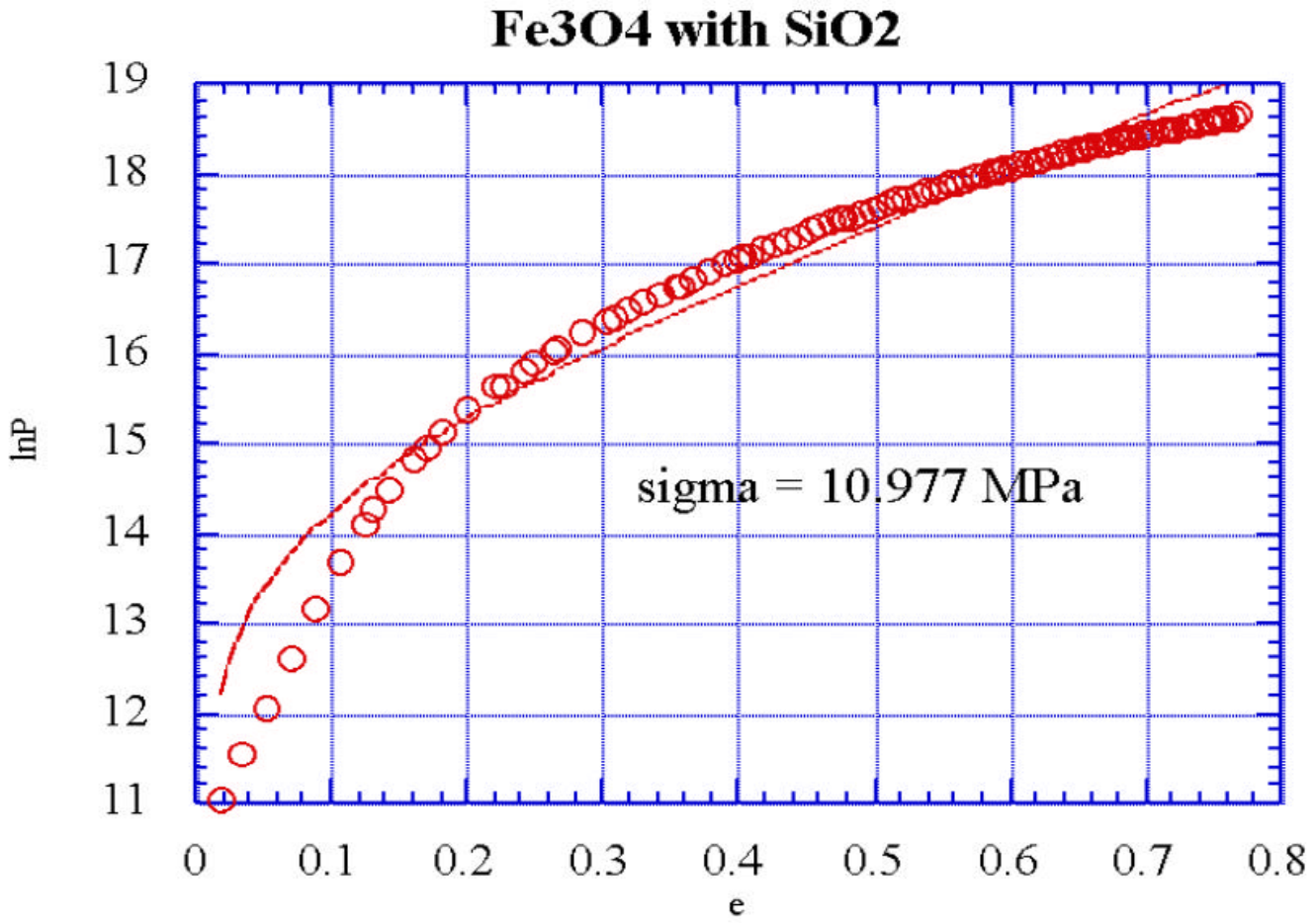

Figure 7 Uniaxial compaction results for the Fe_3O_4/silica catalyst

Appendix A
Characterization of Slurry Phase Iron Catalysts for Fischer-Tropsch synthesis

Linda D. Mansker, Yaming Jin, Dragomir B. Bukur[†], and Abhaya K. Datye[‡]

Center for Micro-Engineered Materials and Chemical and Nuclear Engineering Department
University of New Mexico, Albuquerque, NM 87131-134, USA
[†] Chemical Engineering Department, MS 3122; Texas A&M University,
College Station, Texas
[‡]To whom all correspondence should be addressed

ABSTRACT

The study of Iron Fischer-Tropsch Catalysts by conventional powder X-ray diffraction (XRD) methods is complicated by the multiplicity of phases present (α-Fe, various iron carbides, Fe_xC, magnetite, Fe_3O_4) and by peak overlap in the diffraction patterns arising from these phases. This has led to the consensus that activity for Fischer-Tropsch (F-T) synthesis does not correlate with the bulk composition of the iron catalyst, as seen by XRD. As we show in this paper, some of the problems associated with sample analysis of the working F-T catalyst originate with the difficulty in preserving the microstructures and composition intact, as the sample is prepared for analysis. In this paper, we present analysis of iron F-T catalysts from a stirred tank reactor where samples have been removed under inert atmosphere and care was taken to preserve the catalyst constituents intact. By using XRD with Quantitative Rietveld Structure Refinement (QRSR) analysis, we can construct a comprehensive picture of the working catalyst. These results permit us to explain the activation and deactivation of Fe F-T catalysts and to understand the role of activation method; e.g., CO vs. H_2. We conclude that, in its most active form, the Fe catalyst in a slurry reactor consists of ϵ'-carbide (Fe_7C_3) and alpha-iron (α-Fe), while the χ-carbide, which is also present, appears to be less active. Further work is necessary to elucidate the relative roles of these phases for Iron F-T catalyst activity. Our results also show that Soxhlet extraction, a commonly used procedure to remove the wax from a catalyst, can cause changes in catalyst phase composition.

Introduction

Fischer-Tropsch Synthesis (FTS) of high-molecular weight hydrocarbon waxes from steam-reformed coal is considered an effective solution to the problem of finding suitable substitutes for decreasing liquid fossil fuel reserves. The FTS reaction converts syngas (H_2 / CO) to liquid hydrocarbon feed stocks, which can be used for further processing to chemicals, back-cracked to various API weight fuels, etc. The choice of catalyst depends upon the H_2 / CO ratio. The H_2 / CO ratio is dependent, in turn, upon the syngas precursor and the processing method. A reasonable syngas (H_2 / CO) feed ratio ranges from 1.8 - 2.5. Typically, coals produce an H_2 / CO ratio of 0.5-1.7. For coal-derived syngas, the catalyst must possess adequate water gas shift (WGS) activity to make up the deficit in H_2. In the WGS reaction, one of the FTS products, water (H_2O) and CO from the feed, are converted to H_2 and CO_2, helping to make up the H_2 deficit. Iron catalysts can process the potentially cheaper, lower BTU syngases produced from coals, since they also promote the water-gas shift (WGS) reaction. In this paper, we attempt to describe and quantify the microstructures and composition of two working Fe F-T catalysts obtained from a medium pressure slurry phase reactor.

Iron catalysts, as used for FTS, are prepared by precipitation of a soluble iron species such as $Fe(NO_3)_2$, and calcined to yield hematite (Fe_2O_3). Promoters such as K_2O and CuO, as well as binders such as silica, are also added during preparation. Next, the catalyst is activated outside of the reactor, or it is dispersed in a high molecular weight (C_{30}-C_{40}) hydrocarbon (HC) oil and activated in the reactor. The active iron catalyst is thought to be composed of a mixture of iron oxides (Fe_2O_3, Fe_3O_4), various iron carbides (Fe_xC), and iron metal (α-Fe). There is still no agreement over the nature of the working catalyst and the active phase(s) responsible for F-T synthesis. In the literature, we find studies suggesting that magnetite Fe_3O_4 may be the active phase (Butt, 1981; Teichner, 1982), while other workers concluded that the iron carbides must constitute the active phase (Shroff, 1995, 1996). It is accepted, however, that bulk magnetite introduced into the F-T reactor is inactive for F-T synthesis (Huang et al., 1993) and furthermore, a careful study of catalysts in a fixed bed reactor has clearly linked deactivation of the Fe catalysts to the transformation into magnetite (Coville et al., 1994). These facts would argue against magnetite being the phase responsible for F-T synthesis activity of Fe catalysts. Since the reduced iron phase (α-Fe) tends to carbide to the χ- phase in the syngas atmosphere, it seems likely that, initially, the χ-iron carbide formed should constitute the active phase. However, as shown in this paper, as well as in a companion paper in this special issue (Bukur et al., 1998), a catalyst activated in CO exhibited very low activity initially, despite having almost completely transformed to the χ-carbide phase. Furthermore, this CO-activated catalyst showed a gradual increase in activity to a high steady state value, over a period of time. It would appear that, the presence of iron carbides does not guarantee an active catalyst and some carbide phases may be more active than others. However, previous attempts to relate activity to the carbide phase composition have not been successful, and the review paper by Dry (1980) concluded that there is "no reason to relate the amount and nature of iron carbides to F-T synthesis activity."

In order to gain a better understanding of iron F-T catalysts, we have examined these working Fe catalysts, taking special care to ensure that the catalyst morphology is preserved during sample preparation and subsequent analysis. Careful passivation of these catalysts is very important since the reduced iron phases can readily transform into magnetite upon air exposure (Shroff and Datye, 1995). In this work, the primary analytical technique used was X-ray diffraction. The study was performed as a cooperative effort of two laboratories; the catalyst reactivity study was performed at Texas A&M University (TAMU), while the characterization study was performed at the University of New Mexico (UNM). Specifically, we present an analysis of two runs performed in a stirred tank reactor, using identical catalyst precursor. One of the catalysts was activated in CO at 280° C; the other was activated in H_2 at 250° C. These runs are part of a larger study of catalyst activation treatments conducted at TAMU, as described elsewhere in this issue (Bukur, et al., 1998).

Experimental

The FTS synthesis samples discussed in this paper, from runs SB-3425 and SA-0946, were prepared at Texas A&M University (TAMU) by Dr. Dragomir B. Bukur's research group. Analyses were performed at TAMU and at the University of New Mexico (UNM) from splits. The catalysts used for the runs were prepared from the same precursor. The SB-3425 catalyst was pretreated in H_2 at 250°C, and SA-0946 catalyst in CO at 280°C. The details of catalyst preparation, pretreatment, reaction run conditions, and initial experimental behavior for FTS in a stirred tank reactor are presented elsewhere in this issue (Bukur, et al., 1998).

The product slurry, containing the working catalyst suspended in the product wax, was removed from the CSTR reactor by dip tube, as described in Bukur, et al., 1997. In this study, all samples have been removed under inert atmosphere, in order to preserve the composition and morphologies of the working catalyst sample contained in the hot slurry. The importance of slurry removal under inert vs. slurry removal in air has been discussed elsewhere (Mansker, et al., 1997).

As stated previously, each set of samples were split, and one set of splits provided to UNM for detailed X-ray analysis, by TAMU. X-ray diffraction studies of both sets of the slurry samples and of Soxhlet-extracted powders from SB-3425 were performed at UNM. One slurry sample from SB-3425 was concentrated at UNM, by warming the slurry for several days at 150° C under inert atmosphere and letting the powder concentrate in the bottom portion of the vial. Material was cut from the bottom of the vial and scanned by XRD. The concentrated sample was then completely stripped of its wax under flowing inert at reaction temperature, for subsequent analysis by X-ray diffraction and High Intensity Neutron Powder Diffraction. X-ray scans of Soxhlet-extracted powders from run SA-0946 were performed at TAMU.

The TAMU X-ray diffraction data were obtained using a Scintag XDS2000 series powder diffractometer in fast scan (continuous) mode, Bragg-Brentano (θ-2θ) geometry, 0.02° step size, 1° per minute scan rate. Average diffraction pattern scan error is on the order of 0.05° (0.007 Å). The UNM X-ray diffraction data were obtained using a Scintag PAD-V powder diffractometer with diffracted beam monochromator, operated in step-scan mode, using Bragg-Brentano (θ-2θ) geometry. Scans were taken from either 15° to 105° or 10° to 120° 2θ for each sample, 0.02° per step (SB-3425) or 0.05° per step (SA-0946), 10 s. per step. Average diffraction scan error is on the order of ±0.005° (0.0002 Å). In this paper, however, we will report angles to 2 decimal places, and d-spacings to 3 decimal places.

The UNM step-scan raw data have been used subsequently, for phase identification, structure solution/refinement, minor phase deconvolution, crystallite size analysis, crystallite shape determination, and evaluation of sample preprocessing methods. None of the data were subjected to background, polarization correction, or $K_{\alpha 2}$ stripping, prior to analysis. Slurries, concentrated slurries, and powders were all pack-mounted in a slitted zero-background substrate sample cell, without any preprocessing, addition of solvent, or grinding. Powders in oil were allowed to settle by gravity, then pack-mounted in the same manner as the slurries. Sample volume required was approximately 0.18cc. Precision and accuracy scans were performed using samples from SB-3425.

High Resolution Transmission Electron Microscopy (HRTEM) of samples from runs SB-3425 and SA-0946 was also performed, and the analysis will be discussed in detail elsewhere (Jin, Mansker, and Datye, 1998). We show here a few of the micrographs to illustrate the effects of Soxhlet extraction on the composition of the working catalyst in run SB-3425. The slurry sample was embedded in epoxy, and thin slices on the order of 40-50 nm were prepared using ultramicrotomy. The microtomed section was mounted on a holey carbon film on a molybdenum grid and coated with amorphous carbon to prevent charging. The samples were then examined in a JEOL 2010 HRTEM, operated at 200 KeV. All phase identifications were verified using the diffraction reference data contained in the Joint Committee on Powder Diffraction Standards (JCPDS) powder diffraction data

base, sets 1 to 46, or the single crystal data for the phase, as listed in the International Center for Diffraction Data (ICDD) data base, and in the original papers.

Results

I. Calculated Absolute Powder X-ray Diffraction Intensities of Major Iron Phases

As an important step in the characterization of the Iron Fischer-Tropsch Catalyst by quantitative X-ray diffraction, we will first consider in detail how some of the various observed phases in the working catalyst appear when present in a mixture, and how they may interfere with one another. It is well-known that these materials [e.g., alpha-iron (α-Fe), ϵ'-carbide (Fe_7C_3 or $Fe_{2.2}$ C), χ-carbide (Fe_5C_2 or $Fe_{2.5}C$), and magnetite (Fe_3O_4)] show overlapping diffraction peaks in the region of interest, $\{25° \leq 2\theta \leq 70°\}$. However, most previous analyses, including our own (Shroff, et al., 1995), implicitly assume that the absolute or relative intensities from each phase reflect the relative phase abundances.

All of the standard powder references (JCPDS, ICDD) present the data for each component in terms of relative diffraction intensities, where the most intense diffraction peak is set at 100% relative intensity, and all others normalized accordingly. In principle, the JCPDS database also lists a relative intensity ratio factor for each phase, shown as I/I_{cor} on the card, in which the compound's 100% relative intensity peak is compared to that of corundum (α-Al_2O_3), in a 50:50 wt % mixture. The I/I_{cor} for each phase can then be used to 'correct' the relative peak height ratios commonly used to quantify phases in a mixture, as follows:

$$\frac{w_i}{w_j} = k \frac{I_i}{I_j} \; ; \qquad \textbf{(1)}$$

where W_i , W_j , I_i and I_j refer to the weight fractions and diffraction peak intensities for phases i and j, respectively. The constant, k, is defined in equation 2.

$$k = \frac{(I/I_{cor})_j}{(I/I_{cor})_i} \qquad \textbf{(2)}$$

The use of an experimental I/I_{cor} as a correction factor is based on an assumption that weight percents of the phases in a mixture are nearly equal, and that effects such as preferred orientation, extinction, mixing inhomogeneities, and the breadth of the crystallite size distribution are small enough that the changes in the value of I/I_{cor} are minimal. In the case of the Fischer-Tropsch catalysts, the deviation from equal weight percent mixtures is substantial, intermediate or distorted structures, due to lattice substitutions or vacancies can occur frequently, and if crystallite size is large, preferred orientation becomes a significant problem.

For the iron phases of interest in FTS, the only I/I_{cor} listed in the JCPDS database is that for hematite (α-Fe_2O_3), from a diffraction pattern taken in 1981 (card # 33-664). Due to this paucity of data, we have performed calculations of the powder diffraction patterns to obtain I/I_{cor} for the phases of interest. To confirm the accuracy of this method, we first calculate the pattern for a 50-50 weight % mixture of α-Al_2O_3 and isostructural α-Fe_2O_3, for which phase an I/I_{cor} value is available in the JCPDS, using single crystal structures from the literature (Thompson, et al., 1987 and Antipin, et al., 1985, respectively). Next, we calculate the expected diffraction patterns for a mixture consisting of 20 wt% each of α-Fe, Fe_7C_3, Fe_5C_2, Fe_3O_4, and Fe_2O_3, using single crystal data from the literature (Wyckoff, 1960; Senczyk, 1993; Herbstein and Snyman, 1963; Sénateur, J.P., 1967; Dirand and Afqir, 1983; Fleet, M.E., 1981, 1982, 1984). The calculated diffraction pattern provides a visual indication of the relationship between peak height and sample composition. From these patterns, we can use the I_i/I_j peak ratio and infer an I/I_{cor} using the previously calculated $I/I_{cor}|_{hem}$. The calculations are performed with the DBWS-9411 Rietveld Structure Refinement Program (Young, 1995, Sakthivel and Young, 1995), which lends itself rather well to refinement of X-ray data, and to data simulations. Although not discussed in detail for this paper, neutron diffraction was also performed for one sample from SB-3425 at the Los Alamos Neutron Science Center, and the diffraction pattern is being analyzed using GSAS (Larson and von Dreele, 1997).

Rietveld Refinement is a rigorous polycrystalline powder structure refinement method, first developed by Hugo Rietveld in 1967, for structural analysis of neutron powder diffraction data. Its application to X-ray diffraction data has become wide-spread in the last decade, because it provides detailed information on the structure, morphology, phase abundances, and error in the analytical method, from first principle models of the material of interest. Its rigor also permits diffraction pattern construction on a rather sophisticated scale (Young, 1993). In order to ensure a simulation as close to what we might see in a real, physical analysis, constants describing the instrumental parameters, background function, zero-point error, sample transparency and displacement constants, crystal structure, and crystallite sizes were taken from previous refinements of the slurry and extracted slurry data sets discussed elsewhere in this paper. Further details are available in the literature on the quantification methods used in this analysis (Bish and Howard, 1988; Hill, 1987, 1993).

Figure 1 shows a composite plot of the simulated hematite-corundum mixture. The calculated I/I_{cor} is 2.544. This demonstrates that the calculation procedure yields a value that differs from the experimental value of 2.4 by 6 %. We are assuming that for the next set of simulations, the error in experimental and calculated I/I_{cor} will be comparable in magnitude.

Figure 2a shows the composite plot for the iron phase mixture. The 100% relative intensity peaks for each phase have been labeled. Not only does the figure show the peak overlap that is characteristic of these materials in the region, 25° to 70° 2θ, it also shows that, when absolute intensities are compared, a mixture of the five phases appears to show predominantly α-Fe and Fe_3O_4, with trace amounts of Fe_7C_3, Fe_5C_2, and Fe_2O_3. An I/I_{cor} is calculated for each of the 5 phases, using $I\backslash I_{cor}$ for hematite:

$$\frac{I_i}{I_{cor}} = \frac{I_i}{I_{hem}} \frac{I_{hem}}{I_{cor}} \qquad \textbf{(3)}$$

Table 1 lists the I/I_{cor} calculated, using the simulated patterns in Fig. 2. The numbers in this Table, and the composite diffraction pattern (figure 2a), show that large differences in peak height exist for equal amounts of the various iron phases. These differences must be considered when examining XRD patterns from Fe catalysts used for FTS. It is obvious that a simple examination of relative peak heights could not be used to infer relative amounts of the various phases present in a working catalyst, as will be shown in this work. For completeness, the calculated XRD patterns for each of the phases which make up the 5-component mixture for the second simulation, are included in figures 2b, c, d, e, and f. The detail seen in each of the single-phase plots (2 b-f) is contained in figure 2a, but the different peak heights make it impossible to see this detail. Please note that the structures shown here for the carbides and magnetite are constructed without accounting for phase disorder or distortion, lattice defects, or crystallite preferred orientation, and should be considered as ideal model structures. In the slurry systems, we observe some subtle deviations in details, for the reasons mentioned above.

We next examine a set of FTS catalyst samples from TAMU runs SB-3425, and SA-0946. The activation and initial activities of the materials are discussed in detail elsewhere in this issue (Bukur, et al., 1998). In each case, the slurry samples were split into two portions. One set of splits from each series were forwarded to UNM for analysis by XRD, as described in the experimental section. The other set of splits was retained by TAMU and the catalyst powder separated from the wax by Soxhlet extraction, then analyzed by various methods, including XRD, Mössbauer, and BET (Bukur et al. 1998). After completion of the aforementioned tests, the set of extracted samples and some extracted waxes from SB-3425, were forwarded to UNM for additional analysis. In the next section we describe the effect of Soxhlet extraction on the microstructures of these Fe catalysts.

II. Influence of Soxhlet Extraction on Catalyst Morphology

Characterization of the working catalysts from the slurry reactor is problematic, because of interference from the product wax (discussed in detail in section III) and low initial catalyst loading (on the order of 10% or less). Standard methods of treating this problem have involved using soxhlet extraction to separate the catalyst from the hydrocarbon wax. Unfortunately, this method, which employs solvent at its boiling point (on the order of 80°C, Bukur, 1998), may induce undesirable changes in the powder, as we show here.

We first examine the reduced catalyst sample, in oil (SB-3425, TOS = 0), and compare it to its extracted split., using quantitative X-Ray Diffraction with Quantitative Rietveld Structure Refinement. HRTEM of these two samples was performed, also, to illustrate the kinds of morphology changes which can occur on the microscale, during extraction. Figure 3 shows a comparison of the untreated sample slurry (in oil), and the same sample after soxhlet extraction. The oil is of sufficiently low molecular weight that its 1^{st} and 2^{nd} order diffraction peaks show up as broad, diffuse humps, and can be neglected as background. The same is true of the silica contained in the sample. Visual inspection of the diffraction patterns allows us to make the following observations:

1. The sample in oil contains a prominent peak of α-Fe, along with the characteristic broad, amorphous peaks due to the oil, and the asymmetric, broad peaks with sharp apexes characteristic of amorphous silica. The iron phase appears to have a fairly uniform crystallite

size, as shown by the symmetric, nearly gaussian peak shape, and fairly narrow full-width half maximum (FWHM).

2. The α-Fe peak in the extracted sample is broader, which we attribute to a possible presence of χ-carbide (Fe_5C_2, also known as the Hägg carbide) overlapping with the α-Fe peak. We also see Fe_3O_4 being present, along with α-Fe. The height of the α-Fe peak compared to the background is lower than the sample in oil, indicating a smaller wt % of α-Fe in this sample. The α-Fe peak also shows considerable asymmetry which could arise from a bimodal crystallite size distribution.

Neither χ-Fe_5C_2, nor Fe_3O_4 should have been present, based on the composition observed in the pretreated catalyst in oil. In order to confirm the XRD results, HRTEM of the sample in oil at TOS= 0 hrs and its extracted powder were performed. The micrographs are shown in figures 4, a, b, c, and d.

The HRTEM image of the extracted sample (figure 4a) shows irregularly shaped particles supported on a matrix that contains finer particles. The matrix contains the silica as well as unreduced iron phases. An important feature is the presence of a pronounced surface halo on the particle surfaces, such as that seen on the particles highlighted by arrows in figure 4a. This halo is thicker than a similar surface oxidation layer seen on carefully passivated samples of α-Fe by Shroff and Datye, 1995. A closer examination of one of these haloed particles (figure 4c), shows clearly the thickness of the surface layer, which is on the order of 5 nm, and the irregular particle shape. The particle inner core exhibits lattice fringes of about 2.03Å, which is characteristic of α-Fe (110) planes. Figure 4b and 4d show the TEM micrographs of the TOS = 0 hr slurry sample. The overall microstructure is similar to Fig. 4a and c, but there are no pronounced surface halos on the particle surfaces. These results indicate that either during soxhlet extraction, or after extraction, when the reactive α-Fe surface is exposed to the atmosphere, a surface oxide forms on the primary reduced particles. Figure 4d shows an high magnification view of one of the primary particles indicated by arrow in figure 4b. The particle shape quite irregular, but the surface halo is much thinner. This sample also shows lattice fringes of 2.03Å (α-Fe (110) planes). As we show below, the samples removed after reaction show even more pronounced effects of soxhlet extraction.

We next present the XRD patterns of samples removed from the reactor as a function of time on stream. All of the slurry samples for runs SB-3425 and SA-0946 were analyzed and compared with their soxhlet extracted counterparts. Figure 5a shows the complete SB-3425 slurry series (5 samples), figure 5b shows the complete extracted series SB-3425 (5 samples). Figure 5c shows the complete slurry series SA-0946 (6 samples), and figure 5d shows the complete extracted sample series SA-0946 (6 samples; Bukur, 1998). Note that in figure 5d, the curves are displayed differently, with the end of run sample being the top curve.

Visual inspection of the slurry series, SB-3425, reveals that several peaks remain unchanged with time (figure 5a). We shall demonstrate in section III that these come from the hydrocarbon wax. The extracted samples (figure 5b) show the presence of significant amounts of magnetite, which is clearly <u>not</u> present in the slurry samples. While the presence of wax peaks obscures the location of some of the magnetite peaks in the slurry, the most prominent magnetite peaks indicated in Fig. 5b should

have been observed if magnetite were indeed present in the wax-containing catalyst. Furthermore, the α-Fe peak, which appears consistently in the slurry samples, is completely absent from the extracted samples, except for TOS = 000 hrs. Even in that sample, its intensity is significantly diminished, as shown earlier. The slurry samples show evidence of a shoulder on the right of the α-Fe 100% intensity peak, which is indicative of the presence of ϵ′-carbide, but no evidence of this phase is seen in the extracted samples. The χ-Fe_5C_2 is seen as the most prominent peak in all of the extracted samples. Since the most intense peaks from the χ-Fe_5C_2 are obscured by the wax, it is only after Rietveld refinement of these XRD patterns can we estimate the relative amounts of the Fe phases.

A comparison of the samples from run SA-0946 in slurry and after soxhlet extraction show much less evidence for microstructure changes. It is only the last sample in the series, at TOS=563, which shows pronounced oxidation after soxhlet extraction. The wax appears to interfere much less with the iron phase XRD patterns in this set of samples (figure 5c). Comparing Fig. 5c with Fig. 5a allows one to see clearly that a small amount of magnetite is indeed present in all of the samples from run SA-0946, while no magnetite is present in the working catalyst in run SB-3425. At TOS=000, the sample from run SA-0946 consists of Fe_3O_4 and χ-Fe_5C_2 . As the reaction proceeds, some of the χ-Fe_5C_2 is transformed to ϵ′-Fe_7C_3, the amount of Fe_3O_4 drops, and some α-Fe is observed at TOS = 229, and hrs.

HRTEM of a sample from run SB-3425 at TOS=330 (slurry) and at TOS=384 (extracted) was performed to confirm the XRD observations. The activity of the catalyst at TOS =330 and 384 did not differ very much (refer to section V), and the XRD patterns were also similar. Hence, we can use the TEM images to provide insight into the role of soxhlet extraction, which is the major difference between the sample at TOS=330 and TOS=384.

The soxhlet extracted sample (fig. 5a) shows primary particles of irregular shape all covered with a surface halo. Higher magnification views (fig. 5c) show that these surface layers show lattice fringes consistent with magnetite. The rough surface layer indicates oxidation of the surface has occurred. The sample in wax is shown in Fig. 5b. At low magnification, the morphology is similar to that seen after soxhlet extraction, with similar surface layers. However, at higher magnification (figure 6d), it is clear that these surface layers are amorphous. We have observed that samples removed from a reactor always show such a surface layer (Shroff et al., 1995). We feel that this surface layer is not just a passivation layer caused by surface oxidation, but rather, this amorphous surface layer contains carbonaceous species representing the pool of carbon on the working catalyst. We have found that this pool of carbonaceous species is easy to hydrogenate at reaction temperature (Jackson et al., 1997). While elemental analysis of these surface layers by electron energy loss spectroscopy (EELS) in a TEM could help confirm the composition of these surface layers, such studies need to be performed on samples that have not been exposed to air. We plan to perform such studies in the future, but would like to point out that the crystallinity of these surface layers provides a clear indication of their origins. We have found that while a surface oxide formed at room temperature is often amorphous, beam induced heating during observation transforms it into crystalline magnetite. The lack of crystallinity in the surface layers in Fig. 6d suggests that the amorphous layer does not represent a passivating surface film. The differences between the sample in slurry and after soxhlet

extraction once again indicate that oxidation of the sample occurs either during or after soxhlet extraction.

We conclude that soxhlet extraction of the slurry samples may be undesirable, due the possibility of oxidation, which could occur either during extraction or upon subsequent exposure to air. Evidence for slow oxidation at room temperature despite the protective layer of waxy hydrocarbons is presented in section IV. The oxidation phenomena described here could easily transform highly dispersed α-Fe or carbide phases completely into magnetite. Hence we have focused on the study of catalysts in the wax.

III. Interference of the Crystalline Wax with Catalyst in the Slurry

The wax from a high α-catalyst can be quite crystalline and overlap significantly with the peaks from Fe phases of interest. The diffraction patterns of the wax were analyzed to determine if crystal structure parameters from low-density polyethylene (LDPE) might allow Rietveld refinement methods to be used to deconvolute the wax peaks. Physical methods of separating the wax from the catalyst were also explored and the results are described in this section.

Figure 7 shows six diffraction patterns on the same plot, from run SB-3425, TOS = 233 hrs. From bottom to top, shown are the unprocessed slurry (SL) as removed from the reactor, wax stripped from the slurry by soxhlet extraction (EW), wax stripped from the slurry by warming to reaction temperature (260 C) under flowing inert (SW), catalyst concentrated in the wax by sedimentation, by simply warming at 150°, under inert (CC), soxhlet-extracted catalyst powder (EP), and the powder from which the wax was stripped by flowing inert gas (SP). Comparison of the slurry and the waxes shows that the wax accounts for many of the diffraction peaks present in the slurry, and thus could be easily misidentified as iron phases, as is evident from the peak positions listed in Table 2.

A visual inspection of the slurry pattern shows a prominent α-Fe peak that occurs at 44.78° 2θ. The neutron diffraction pattern (not shown here) also identifies α-Fe as the major peak in the stripped powder. However, in view of the high I/I_{cor} for α-Fe, it should be emphasized that significant amounts of carbide are also present in this sample, as discussed below (section V). Most remarkable is the difference between the stripped powder (SP) and the soxhlet-extracted powder (EP). The α-Fe peak is completely missing and is replaced by a broad magnetite peak. A large χ-carbide peak is seen to be the major constituent of the EP, but the Rietveld refinement results of the stripped powder (SP1) in section V suggest that the catalyst contains only α-Fe and ε'-carbide. It is clear that a study of soxhlet extracted powders would not be very useful for understanding working Fe catalysts in a F-T synthesis reactor.

Comparison of the slurry catalyst with either of the wax diffraction patterns shows that regions of 2θ exist, where no wax peaks interfere with iron phase diffraction peaks. Keeping this in mind, we look for additional detail in the region between 52° and 67° 2θ. Fe_3O_4 has two moderately intense peaks which occur at 57° and 62.5°. α-Fe has peaks at 44.78° and 65.00°. χ-Fe_5C_2 and ϵ′-Fe_7C_3 both have 100% relative intensity peaks which overlap with the α-Fe 100% relative intensity peak, in the range 44° - 45°, at 44.175° and 44.882° 2θ, respectively, but are clear of the wax phase. χ-Fe_5C_2 has a

fairly intense peak at about 50.48° (~ 12 %), and ϵ'-Fe_7C_3 at 25.9° (~ 12%), but, again, the relative intensity ratios with α-Fe and magnetite are such that visual inspection for these phases becomes difficult.

The catalyst crystallite sizes are small enough (≈ 15 nm) and relative intensity ratios such that significant overlap can occur (cf. Section I, table 2, figure 2). Presence of either of the carbides, in the presence of α-Fe, can be detected by examining the α-Fe peak shape. The α-Fe crystallites in the unprocessed slurry produce a nearly Gaussian peak shape. Asymmetries in the 100% intensity peak shape, especially in the tail, are indicative of other phases present, where appearance of a shoulder or 'bumpy' tail to the left suggests χ-Fe_5C_2, and where presence of a 'bumpy' asymmetry on the right indicates ϵ'-Fe_7C_3. Using this criterion, we have ascertained that ϵ'-Fe_7C_3 is present in the slurry, but that, in this sample, χ-Fe_5C_2 is not. In summary, qualitative analysis of the catalyst in the slurry shows the presence of α-Fe and ϵ'-Fe_7C_3 but no magnetite to be present in the slurry. While the α-Fe peaks occur at 2θ values where there is no overlap with the wax diffraction peaks, some of the carbide peaks do overlap, making it difficult to perform quantitative Rietveld Structure Refinement (QRSR). Accordingly, a study of the wax was made, using a structure model, and two slurry samples refined for phase identification, in order to test the effectiveness of using QRSR on a highly crystalline wax slurry sample.

A question arose, regarding entrainment of small crystallites of catalyst in the wax because the two waxes (EW and SW) differ in subtle details and in color, neither being clear or white. Consequently, before QRSR analysis of the slurry was attempted, 10 mg each of the extracted wax and inert-stripped wax were digested and analyzed by atomic emission spectroscopy. The extracted wax(EW) showed a total iron content of 80 ppm, and the stripped wax (SW) a total iron content of 207 ppm. Both are well below our detection limit of 350 ppm for XRD, so we concluded that iron entrained in the separated wax does not contribute significantly to the wax diffraction pattern. The wax was subsequently refined, using the polyethylene crystal structure of Hu and Dorset, 1989. We obtained a fairly good fit, with high crystallinity.

IV. Quantitative Rietveld Refinement, and Precision and Accuracy

The refined structure parameters were used to deconvolute the wax product diffraction pattern from the slurry. Refinement of the SB-3425 slurry sample from TOS = 233 hrs was attempted first, because visual inspection indicated the presence of α-Fe and ϵ'-carbide. Earlier in this discussion it was mentioned that the diffraction peaks for α-Fe all fall clear of the wax in the angle range (40° - 120° 2θ); recalling also, from section I, that it appears that the diffraction intensity of α-Fe relative to ϵ'-carbide is 3 orders of magnitude higher, we refined for the wax and for α-Fe only, which would leave ϵ'-carbide in the residual, if truly present.

The results are shown here as figure 8a. After a rough refinement for the waxy product and α-Fe, a somewhat noisy diffraction pattern, which contains residual wax peaks with some as-yet unidentified iron phases emerges (bottom curve, figure 8a). Because the residual peak intensities, in many cases, are of the same order of magnitude as the background, visual identification may be difficult. In the case of the second slurry sample, from run SA-0946, TOS = 0, there is no highly crystalline product present, only C40 oil. Additionally, since, by visual inspection, magnetite and χ-

carbide are considered present, and their raw diffraction intensities are comparable, we refined for both phases. Figure 8b shows the complete refinement. Further refinement of the residual from figure 8a, and the quantification for both samples, is discussed in section VI.

Periodically, some samples were reanalyzed to verify the repeatability and accuracy of our analytical technique, and to check sample stability in the slurry. We have decided to evaluate two of these repeated samples, SB-3425, TOS = 384 hrs, slurry, and SB-3425, TOS = 233 hrs, wax stripped powder. The slurry sample from SB-3425, TOS = 384 hrs has been analyzed twice, 7 months apart. The diffraction patterns are shown here as figure 9a. They appear identical, except that the α-Fe peaks, present in the first scan at 44.8° and 65.00° 2θ, are not present in the same sample, 7 months later. In fact, the second scan appears little different than the wax diffraction patterns shown in figure 7. Upon applying Quantitative Rietveld Refinement to the repeat, using the two LDPE model structures used to deconvolute the waxes, we determined that the only catalytic component phase still present was a very disordered, crystalline magnetite, of small crystallite size (Mansker and Datye, 1998). The previous results make it clear that the iron catalyst is so reactive, that it undergoes changes, even in the wax matrix.

We analyzed the wax-stripped powder, from SB-3425, TOS = 233 hrs, in order to determine if the catalyst composition was as much affected by wax removal under flowing inert at reaction temperature, as it appeared to do upon soxhlet extraction. It was first subjected to a neutron diffraction (ND) study, scanned by XRD 1 month later, then scanned by XRD, again, 4 months after the ND study. We will not discuss the details of the diffraction analysis interpretation or the Quantitative Rietveld Structure Refinement here (see Mansker and Datye, 1998), results indicated that, although the major peak seen in the sample can be easily identified as α-Fe, the phase compositions in the sample could be summarized as a mixture of α-Fe, with ϵ'-carbide (ND and XRD) and trace magnetite (XRD).

As a quality control check, the stripped powder sample was X-rayed again, 3 months later, in order to determine its stability. Both samples are shown in figure 9b. Visual inspection of the two diffraction patterns shows that subtle changes have taken place. The intensity of the iron peak has diminished somewhat after 4 months, and some of the minor phase peaks have become more prominent. All the peak widths are broader, indicating crystallite breakup has occurred. Rietveld refinement of the diffraction data for the repeat also indicated that the sample composition had changed again. More of the sample had oxidized, the volume average crystallite sizes had decreased (e.g., the peaks widths had increased), and the ϵ'-carbide had completely transformed to the more stable χ-carbide !

The analysis of the wax-stripped powder shows that, even when care is taken to protect the powder from air, when wax removal is attempted, and afterward, the catalyst remains highly reactive. We conclude that the Iron Fischer-Tropsch catalyst, contained in the product wax, can provide an accurate picture of the working catalyst, but only if analyzed in a timely manner. It appears that physically stripping the wax under flowing inert, or with a combination of suitable solvents (but at room temperature) may provide samples with improved signal to noise ratio for quantitative analysis. Work is in progress in this regard.

V. Fischer-Tropsch Reaction Results

Reactivity data for the catalysts studied here, runs SB-3425, and SA-0946, are included here as figure 10. Instead of showing % conversion, we have shown the apparent first order rate constant which provides an accurate picture of the intrinsic reactivity of the catalyst. The % conversion was generally high (80%) and is affected by changes in flow rate as well as reaction temperature. The data here have been normalized to a reaction temperature of 250 C. Actual conversions for these runs are shown in the companion paper by Bukur et al. (1998). Table 3 shows the process parameters during these runs as a function of time and % conversion at selected times on stream.

The catalyst prepared for run SA-0946, activated in CO at 280°, shows a lengthy induction period, in which the activity starts very low and then rises steadily to its steady state value. SB-3425, activated in H_2 at 250°C, shows high activity at the outset. However, its activity begins to fall at longer run times. The SA-0946 run reaches steady state activity near TOS = 113 hrs, where a slurry sample was obtained. Its steady state activity is higher than that of SB-3425, and shows stable activity with time, with some fall off in activity towards the end of the run. In the next section, we will relate these observed variations in catalyst activity with the phase composition and morphology.

VI. Catalyst Evolution with Time on Stream

We have implied, in the previous sections, that the catalyst shows subtle, but definite phase changes which correlate with the changes in the activity profiles, in each run. We will now describe these changes in detail, and discuss what these changes tell us about the catalyst's active components, over time. We will contrast the behavior of the catalyst in two runs: SA-0946, and SB-3425. Samples from run SA-0946 were removed from the reactor at TOS = {0, 113, 229, 354, 427, and 563} hrs. Samples from run SB-3425 were removed from the reactor at TOS = {0, 111, 233, 330, and 384} hrs. XRD patterns from these runs have been presented as figures 5a, b, c, and d, respectively. Since we have already documented the changes in phase composition caused by soxhlet extraction, we will restrict our analysis to the slurry catalyst samples.

Now, we present the results of the quantification of the slurry and extracted samples from runs SB-3425, and SA-0946, using Quantitative Rietveld Refinement, or the estimated I/I_{cor} with the peak intensity, as observed in the diffraction pattern. Table 2 contains the data from the slurry samples, SB-3425, including a powder obtained from stripping under inert atmosphere (sample SP1; ref. Section IV).

Two consistency tests were used. First, weight percents at TOS = 111 hrs were calculated using the estimated I/I_{cor} and the 100% peak heights, and by the more rigorous Rietveld method. The results are in good agreement with one another. The second consistency test involved TOS = 233 data, which shows some self- consistency between the slurry, and the powder obtained by wax-stripping under flowing inert (SP1). Recall, from section III, that the stripped powder was first subjected to a neutron diffraction study, scanned by XRD 1 month later (SP1), then scanned again 3 months after that (SP2). Stripping of the wax improves the signal considerably as seen from Fig. 7. The high intensity of scattering from the α-Fe phase, as manifested in the I/I_{cor} values reported in table 1, means that the carbide peak will be difficult to see when the α-Fe is present. This factor is responsible for

the major uncertainty in composition and crystallite size in these refinements. We propose to corroborate these values in future work by using Mossbauer spectroscopy and neutron diffraction. The X-ray scattering cross sections for carbon and iron are very different, making it difficult to 'see' the compounds with significant carbon content in a mixture, by X-ray. Under neutron diffraction, the scattering cross sections are of the same order of magnitude; this means that the latter technique may be more sensitive to the carbide phase in the presence of α-Fe.

Referring the reader back to figure 10, we will now discuss the activity curve for SB-3425. Initially, the crystallite size for TOS = 000 hrs, α-Fe, is on the order of 13.5 nm which is in reasonable agreement with the TEM image reported in Fig. 4. The catalyst appears to transform quickly into ϵ′-carbide and at TOS = 111 hrs, our refinement suggests that it is almost completely transformed into the carbide phase. At this stage, the crystallite sizes for α-Fe are about 37.9 nm, with ϵ′-carbide at about 5.5 nm. The catalyst is active until approximately TOS = 160 hrs, when a fairly sharp drop-off occurs. Coincidentally, there was a change in experimental conditions: a decrease in space velocity. While the phase composition of the catalyst remains the same, we observe an increase in crystallite size for ϵ′-carbide and a slight decrease in that for α-Fe in the sample at 233 hours. The crystallite size for α-Fe was about 30 nm, while that for ϵ′-carbide was estimated to be 47 nm. When the wax was stripped from the catalyst by heating under flowing inert at 270 C, the XRD analysis of the resulting powder shows comparable crystallite size. The next sample, withdrawn at TOS=330 hours, shows a major change in phase composition. The catalyst now contains 86% χ-carbide with only 14% ϵ′-carbide. The particle sizes are now 37.2 nm for α-Fe and 7.6 nm for χ-carbide.

This number can be compared with the particle size of about 25 nm from the TEM image in Fig. 4a and it is clear that the agreement is not very good. One possible explanation is that XRD is sensitive to the size of the crystalline domains while TEM sees the entire particle. Hence, if the particles are not single crystals, the XRD estimate of particle size will be smaller than the TEM size. Many of the particles in Fig. 4a are clearly not single crystals. High resolution images such as the one in Fig. 4c show the lattice planes in the crystal and allow us to identify the phase if individual crystals. However, the average phase composition is more difficult to estimate from TEM since it would involve high resolution imaging of numerous crystallites and matching the lattice planes with the expected spacings for each phase. Our limited survey of these particles indicated that the majority of them showed lattice fringes of 2.13 A which would be consistent with the presence of the χ'-carbide. Hence, the TEM is in qualitative agreement with results of the Rietveld refinement as regards phase composition. By TOS=384, the catalyst appears to have transformed almost completely into the χ-carbide, by XRD. The doubling of the crystallite size seen by XRD is again not seen in the TEM images, but this is subject to the uncertainties in XRD crystallite size estimates described above.

The significant crystallite size growth, and corresponding loss of surface area in the ϵ′-carbide phase may explain the drop in activity which occurs early in this run. The processes responsible for the observed transformation from ϵ′-carbide to the χ-carbide need further study. The loss of activity in this catalyst appears related to the loss of the α-Fe and ϵ′-carbide and the growth of the χ-carbide by TOS = 330. If, as we contend, α-Fe and ϵ′-carbide are necessary components of an active catalyst, and χ-carbide is less active for FTS, the appearance and increase in χ-carbide, with the concurrent decrease in the remaining two phases is also consistent with the drop in activity. As a further check,

although not listed in the table, the relative amounts of wax were monitored in the sample series. Keeping in mind that these are **weight** percents, and that the waxy product distribution could have, on average a molecular weight (MW) of at least 3000 g/mole, Rietveld refinement of the slurries, using two LDPE model structures with MW of 3000 and 1500, respectively, with some disorder, gave a total organic weight percent of 99.98%, for all four samples, TOS = {111, 233, 330, and 384} hrs, with a breakdown of about 35 % material at 3000 g/mole, and 65% material at 1500 g/mole.

Table 5 contains the composition and crystallite size data for SA-0946, slurry series. For SA-0946, the initial slurry sample (TOS = 000 hrs) consists mainly of χ-carbide, ϵ'-carbide, and trace magnetite in the ratios 13.41 : 86.38 : 0.22, or essentially, a carbide ratio (χ:ϵ') of 6.44, with corresponding volume average crystallite sizes of about 27.0 nm and 13.7 nm, respectively. By TOS = 113 hrs, a major phase transformation has occurred wherein the χ-carbide has converted to the ϵ'-carbide. The ratio of these carbides is now 1.14:1, with corresponding crystallite sizes of 11.6 nm and 11.4 nm, respectively. Referring back to figure 10, this coincides with a maximum in the activity versus time curve for this run. After TOS 113 hrs, the activity shows a mild drop and then the activity is relatively constant. The activity begins to drop off again at TOS = 563 hrs. Carbide ratios remain around 1:1, until the sample withdrawn at TOS = 427 hrs, where the ratio increases to 4.47:1. Crystallite size for the carbides is also growing slowly for both carbides until after 427 hrs when the χ-carbide crystallite size increases to 3.5 times that of the ϵ' phase. There is only a trace of α-iron or of magnetite, although both appear significant, from visual inspection of the XRD patterns. It should be remembered that Table 2 has shown that the phases that scatter most strongly are α-Fe and magnetite, hence their peaks are disproportionately larger than their abundances. The amount of magnetite seems to increase slightly towards the end of the run, with a crystallite size much greater than that of the carbide phases.

We conclude that the transformation of the χ-carbide into ϵ'-carbide, and a corresponding break up in crystallite size, are both responsible for the slow activation of this CO activated catalyst. The mild deactivation towards the end of the run seems to be caused by an increase in the χ-carbide/ϵ'-carbide ratio, and an increase in crystallite size.

Summary

This work reports a careful study of the XRD patterns of working Fe based catalysts. These catalysts were used for a Fischer-Tropsch reaction run under conditions similar to those used for commercial FT synthesis. Care was taken during sample withdrawal to protect the hot wax against atmospheric oxidation. The objective of this study was to quantify the relative amounts and the crystallite sizes of the phases present in the reactor as a function of time. Since the XRD databases do not report absolute intensities of the diffraction peaks, we performed a calculation to determine these intensities. The relative peak heights for a 20 wt% mixture of the various Fe phases were reported in Table 1 with respect to corundum, a standard used in XRD analyses. Based on Table 1, we can derive relative peak heights as follows: (α-Fe = 5440; Fe_3O_4 = 487; Fe_7C_3 = 11.5; Fe_2O_3 = 8.7; Fe_5C_2 = 1). The variation of over three orders of magnitude implies that a simple visual examination of peak heights in this system is very deceptive. In a mixture of these phases, the α-Fe or the magnetite peaks will stand out most prominently. Furthermore, the catalyst is so reactive to oxygen in its reduced state that unless great care is exercised, the reduced α-Fe species can transform into magnetite.

Hence, one would expect magnetite to be the most prominent phase seen in XRD patterns, as seen in reviews of previous literature. However, magnetite is not the major constituent of slurry phase Fe catalysts: in these runs we found total magnetite content to be less than 1 wt%. This study also shows that soxhlet extraction, a commonly used procedure for removing the wax from the catalyst, can result in phase transformations in the catalyst. The phase transformations can occur during extraction, or upon subsequent air exposure. It is also possible that the hot solvent may react with the reduced species, particularly with α-Fe. In view of these potential complications, we examined the catalysts directly in the hydrocarbon wax.

We found that the hydrocarbon wax can be quite crystalline, particularly from a high alpha catalyst, and the wax interferes quite extensively with the Fe phases of interest. Physical means of separating the wax were explored. Heating the wax in flowing inert gas at reaction temperature caused most of the wax to entrain and flow out with the gas, leaving behind the catalyst powder. The wax peaks were practically eliminated in this process, but there remains the concern that the heat treatment may cause changes in catalyst structure. In future work, other methods to remove the wax interference in XRD patterns need to be explored.

Quantitative Rietveld Structure Refinement was performed for the wax-containing catalysts from two F-T runs. These runs had differing activation procedures and showed dramatically different activity profiles. The Rietveld refinements of the H_2-activated catalyst SB-3425 have the greatest uncertainty since the dominant peaks in the XRD pattern come from the wax. These wax peaks completely obscure the most intense peaks from χ-carbide, but the α-Fe and magnetite peaks can be clearly seen. We can state conclusively that the working catalyst in this run does not show the presence of any magnetite. Our refinements suggest that in its initial state, the catalyst contains a mixture of α-Fe and ϵ'-carbide. The drop in activity is caused by a growth in ϵ'-carbide crystallite size, and later in the run, a transformation of the ϵ'-carbide into χ-carbide.

The refinement of the XRD patterns from the CO activated catalyst SA-0946 is easier since the wax peaks are less pronounced. The CO-reduced catalyst, at TOS = 000 hrs, contains χ-carbide, with a smaller amount of ϵ'-carbide. No graphite is seen by XRD and TEM images show only a small fraction of the carbide particles to be covered by graphite. This catalyst exhibits a low activity, initially, which increases to a steady state value, with a concomitant break up into ***smaller*** crystallites, and a decrease in the carbide ratio, which we define as the ratio of ($\chi : \epsilon'$) carbide. As long as the carbide ratio and crystallite size remains fairly constant *and* small, the activity remains high. Activity appears to decrease with increasing carbide ratio, and with increased crystallite size.

This work has also illustrated that microtomy can be used to prepare thin sections of the working catalyst in wax for analysis by TEM. HRTEM data provide useful corroboration of the phase identification by XRD, providing a detailed picture of the relationship between the microstructure of a working Fe catalyst with its catalytic reactivity. Detailed HRTEM observations of a series of Fe catalysts will be presented elsewhere (Jin et al., 1998). Future work will attempt a correlation of the XRD refinements with Mossbauer spectroscopy and neutron diffraction. Comprehensive analysis by HRTEM should allow determination of the surface areas of the various phases and the role of these phases in determining the activity and selectivity of Fe F-T catalysts.

Conclusions

The following conclusions can be drawn from this study:

- Fe catalysts that have been soxhlet extracted show evidence of oxidation and possible phase transformations (α-Fe to χ-carbide), hence it is preferable to rely on analyses of the catalyst in the hydrocarbon wax.

- The hydrocarbon wax can be quite crystalline, particularly with a high α catalyst, resulting in severe interference with several of the peaks from the Fe phases of interest. Future work needs to be directed to methods to reduce the interference from the wax.

- The absolute intensities of the diffraction lines from the various phases differ by over three orders of magnitude. This means that a visual examination of peak heights from an XRD pattern provides no clues to the relative abundance of the various phases present.

- Analysis of XRD patterns must be conducted using Rietveld Structure Refinement methods. The accuracy of these refinements will depend on signal to noise ratio (increased catalyst loading relative to the wax). In this regard physical means to concentrate the catalyst seem necessary.

- When the catalyst activated in H_2 at 250 C was used for F-T synthesis, it was found to transform readily into a mixture of α-Fe and ϵ'-carbide, in which form it was as active as the best catalysts prepared by CO activation. The catalyst lost activity due to a conversion into χ-carbide and growth in crystallite size.

- In contrast, a catalyst activated in CO was initially composed of a mixture of χ-carbide and ϵ'-carbide with a carbide ratio (χ:ϵ') of 6.44 In this state, the catalyst showed very low activity. Increase in activity was accompanied by a decrease in the carbide ratio as well as a break up into smaller-sized particles. The modest deactivation of this catalyst seen towards the end of the run seems to coincide with a transformation of the ϵ'-carbide into χ-carbide.

- This study clearly suggests that the ϵ'-carbide in combination with α-Fe is associated with the most active catalysts while χ-carbide appears to be less active. Further work is necessary to understand the driving force for these phase transformations, and the relative contributions from the these phases to overall F-T activity and selectivity. The XRD quantitation needs to be corroborated with TEM, Mossbauer and neutron diffraction to provide an accurate picture of the relative amounts and particle sizes of the different phases present in a Fe F-T synthesis reactor.

Acknowledgments

This work was supported under the U.S. Department of Energy University Coal Research Grant DE-FG22-95PC95210, with partial support from NSF HRD 93-53208 at the University of New Mexico, and by U. S. Department of Energy Contract DE-AC22-94PC93069 at Texas A&M University. We

further acknowledge the X-ray Powder Diffraction Laboratory, Department of Earth and Planetary Sciences, University of New Mexico, and Los Alamos National Laboratory, Manuel Lujan Neutron Scattering Center.

References

Amelse, J.A.; Schwartz, L.H.; and Butt, J.B.; Journal of Catalysis; **72**, 95 (1981).

Antipin, M.Iu.; Tairelson, V.G.; Flugge, M.P.; Gerr, R.G.; Struchkov, Iu. T.; and Oserov, R.P.; Doklady Akadameii Nauk SSSR; **281**(4); 854 (1985).

Baltrus, J.P; Diehl, J.R.; McDonald, M.A.; and Zarochak, M.F.; Applied Catalysis; **48**, 199 (1989).

Bish, D.L. and Howard, S.A.; Journal of Applied Crystallography, **21**, 86-91 (1988).

Blanchard, F.B.; Raymond, J.P.; Pommier, B.; and Teichner, S.J.; Journal of Molecular Catalysis; **17**, 171 (1982).

Bukur, D.B.; Nowicki, L.; and Lang, X.; Catalysis Today; **24**; 111 (1995).

Bukur, D.B.; Lang, X.; and Ding, Y.; Preprints of the American Chemical Society Division of Fuels Chemistry; **42**(2); 623 (1997).

Bukur, D.B; Lang, X.; and Ding, Y.; Applied Catalysis, this issue (1998).

Dictor R.A.and Bell, A.T.; Journal of Catalysis; **97**, 121 (1986).

Dirand, M. and Afqir, L.; Acta Metallurgica; **31**(7); 1089 (1983).

Dry, M.E.; 'Catalysis - Science and Technology'; J.R. Anderson and M. Boudart, Eds.; Chapter 15, 160 (1980).

Duvenhage, D.J.; Espinoza, R.L.; and Coville, N.J.; Studies in Surface Science and Catalysis; **88**; 351 (1994).

Dwyer, D.J. and Somorjai, G.A.; Journal of Catalysis; **52**, 291 (1978).

Fleet; M.E.; Acta Crystallographica, **B37**, 917 (1981).

Fleet, M.E.; Acta Crystallographica, **B38**, 1718 (1982).

Fleet, M.E.; Acta Crystallographica, **C40**, 1491 (1984).

Herbstein F.H. and Snyman, J.A.; Inorganic Chemistry, **3**(6), 894 (1964).

Hill, R.J.; and Howard, C.J.; Journal of Applied Crystallography, **20**, 467-474 (1987).

Hill, R.J., in the 'The Rietveld Method'; Young, R.A., ed.; International Union of Crystallography, Oxford University Press, Pub.; 61-101 (1993).

Hu, H.L. and Dorset, D.L.; Acta Crystallographica; **B45**, 283 (1989).

Huang, C.S.; Xu, L.; Davis, B.H.; Fuel Science and Technology, International. **11**; 639 (1993).

Jager, B and Espinoza, R.L.; Catalysis Today; **23**; 17 (1995).

Jackson, N. B., Mansker, L. D., O'Brien, R. J., Davis, B. H. and Datye, A. K., Studies in Surface Science and Catalysis, **111**, 501, (1997).

Jin, Y., Mansker, L.D., and Datye, A.K., in preparation for submission to the Natural Gas Conversion meeting, Taornimo, Italy, September 1998.

Kalakkad, D.S.; Shroff, M.D.; Köhler, S.D.; Jackson, N.B.; and Datye, A.K.; Applied Catalysis A; **133**; 335 (1995).

Larson, A.C. and Von Dreele, R.B.; "GSAS: General Structure Analysis Program"; Los Alamos National Laboratory, Los Alamos, NM 87545(1997).

Mansker, L.D., Jin, Y.; and Datye, A. K.; Proc. Coal Liquefaction and Solid Fuels '97 Conference proceedings, electronic publication, Federal Energies and Technologies Center, Pittsburgh, Pennsylvania; http://www.fetc.doe.gov/events/97conferences/coal_liq/97cl_pdf/datye.pdf/; (1997).

Mansker, L.D. and Datye, A.K.; in preparation, 1998.

McCartney, J.T.; Hofer, L.J.E.; Seligman, B.; Lecky, J.A.; Peebles, W.C.; and Anderson, R.B.; Industrial and Engineering Chemistry; **57**; 730; (1953).

Niemantsverdriet, J.W.; van der Kraan, A.M.; van Dijk, W.L.; and van der Baan, H.S.; Journal of Physical Chemistry; **84**(25); 3363 (1980).
Niemantsverdriet, J.W.; and van der Kraan, A.M.; Journal of Catalysis; **72**; 375 (1981).
O'Brien, R.J.; Xu, L.; Spicer. R.L.; Bao, S.Q.; Milburn, D.R.; and Davis, B.H.; Catalysis Today; **36**(3); 325 (1997).
Rath, L.K. and Longanbach, J.R.; Energy Sources; **13**; 443 (1991).
Raupp, G.B. and Delgass, W.N.; Journal of Catalysis **58**, 348, (1979).
Rao, V.U.S.; Stiegel, G.J.; Cinquegrane, G.J.; and Srivastava, R.D.; Fuel Processing Technology; 30; 83 (1992).
Rao, Huggins, Huffman, Gormley, O'Brien, and Davis, Energy and Fuels; b; 546 (1996).
Rao, K.R.P.M.; Huggins, F.E.; Huffman, G.P.; Gormley, R.J.; O'Brien, R.J.; Davis, B.H.; Energy and Fuels; **10**(3); 546 (1996).
Sakthivel, A. and Young R.A.; Rietveld Analysis Program DBWS-9411, Release 30.03.95, software, (1995).
Sénateur, J.P.; Annales de Chimie, **2**, 103 (1967).
Senczyk, D.; Phase Transitions, **43**, 153 (1993).
Shroff, M.D.; Kalakkad, D.S.; Coulter, K.E.; Kohler, S.D.; Harrington, M.S.; Jackson, N.B.; Sault, A. G.; and Datye, A.K.; Journal of Catalysis, **156**(2), 185-207 (1995).
Shroff, M.D.; Datye, A.K; Catalysis Letters, **37** (1-2); 101-106 (1996).
Thompson, P; Cox, D.E.; and Hastings, J.B.; Journal of Applied Crystallography, **20**, 79 (1987).
Wyckoff, R.W.G; New York, 3rd Ed.; Interscience Publishers, 1960.
Young, R.A., ed.; 'The Rietveld Method'; International Union of Crystallography, Oxford University Press, Pub.; (1993).
Young R.A.; Journal of Applied Crystallography, **28**, 366-367 (1995).

Figure Captions

Figure 1 Simulated X-ray diffraction pattern of a 50:50 wt % mixture of hematite (Fe_2O_3) and corundum (α-Al_2O_3). The peak height ratio for the 100% peaks, $I/_{Icor}$, is 2.544.

Figure 2 a) Simulated X-ray diffraction pattern for a 20 wt% mixture of each of these phases: Fe_2O_3:Fe_3O_4:α-Fe:Fe_7C_3:Fe_5C_2 ; The remaining plots represent the simulated pattern for each of these phases plotted at full scale: b) Fe_2O_3 c) Fe_3O_4 d) α-Fe e) Fe_7C_3 f) Fe_5C_2.

Figure 3: X-ray diffraction pattern from run SB-3425, TOS = 000 hrs. Lower curve, sample in the oil, and upper curve: powder after soxhlet extraction .

Figure 4
- a: Low magnification view of SB-3425, TOS = 000 hrs, extracted powder
- b: Low magnification view of SB-3425, TOS = 000 hrs, slurry
- c: High magnification view of SB-3425, TOS = 000 hrs, extracted powder
- d: High magnification view of SB-3425, TOS = 000 hrs, slurry

Figure 5
- a: X-ray diffraction of samples from run SB-3425, slurry samples
- b: X-ray diffraction of samples from run SB-3425, extracted samples
- c: X-ray diffraction of samples from run SA-0946, slurry samples
- d: X-ray diffraction of samples from run SA-0946, extracted samples. Note the loss of preferred orientation in the χ-carbide phase, with increasing TOS (*except* in TOS = 563) - this indicates that the particles are breaking up. The samples show significant zero-point error, as an S-shaped displacement in the peaks, with TOS. This probably arises from sample prep error, and could not be corrected for directly by UNM, due to lack of access to the raw data. Thus, labeling has been based on the reference angles and/or easily recognizable peak-group shapes.

Figure 6
- a: Low magnification view of SB-3425, TOS = 384 hrs, extracted powder
- b: Low magnification view of SB-3425, TOS = 330 hrs, slurry
- c: High magnification view of SB-3425, TOS = 384 hrs, extracted powder
- d: High magnification view of SB-3425, TOS = 330 hrs, slurry. Note that figure 5c shows images of the powder, without embedding in epoxy and microtomy.

Figure 7 X-ray diffraction of sample taken at TOS = 233 hrs, run SB-3425 concentrated by physical means. Original slurry, soxhlet extracted wax, stripped wax (by heating under flowing inert), catalyst concentrate prepared by sedimentation, catalyst after soxhlet extraction and catalyst after the wax was stripped off in flowing inert. The α-Fe peak seen in the slurry sample grows in size as the catalyst is concentrated, while the wax peaks diminish in intensity. Note the remarkable difference between the soxhlet extracted powder and the inert-stripped powder.

Figure 8
- a: Incomplete Rietveld refinement of SB-3425, TOS = 233 hrs, for wax (LDPE structure) and α-Fe. The residual, although extremely noisy, contains the remaining ϵ'-carbide. The residual also shows a few additional peaks from the wax, originating with the lower molecular weight component and its extreme disorder.
- b: Rietveld refinement of SA-0946, TOS = 000 hrs, catalyst in oil, for magnetite, χ-carbide, and ϵ'-carbide . Note the relative lack of significant diffraction

intensity in the residual curve, except for the oil and amorphous silica. This diffraction pattern also shows some trace hematite (sharp spikes).

Figure 9 a: XRD plot of SB-3425, TOS = 384 hrs, slurry, repeat analysis after a 7 month period where the catalyst sat in the laboratory exposed to air. The α-Fe peak has disappeared despite the presence of the wax which encapsulates the catalyst. The magnetite that forms is poorly crystalline and therefore does not show up in the XRD pattern.

b: XRD plot of SB-3425, TOS = 233, stripped powder repeat analysis after 3 months. It appears that the wax residue left after heating the catalyst in flowing inert does a better job of protecting the catalyst from further oxidation.

Figure 10: Fischer-Tropsch reactivity for runs SB-3425, and SA-0946. The results are plotted in the form of a pseudo first order rate constant referenced to 260°C. The rate constant is in mmol of CO converted per g Fe per Mpa pressure per hour. The reactor was operated at temperatures ranging from 260 C to 266 C and varying space velocities. The process conditions and actual conversion at several times on stream are shown in Table 3.

Table 1: I/I_{cor} for iron phase mixture		
Phase	**Imax**	**$I\backslash I_{cor}$, calculated**
Fe	5.750E+05	1592.3
FE_7C_3	1220.	3.378
Fe_5C_2	105.7	0.293
Fe_3O_4	5.1458E+04	142.50
Fe_2O_3	919.1	2.544

Table 2: d-spacings, angles, and relative intensities in the Wax XRD							
d-spacing, Å	**2.986**	**2.569**	**2.545**	**2.485**	**2.108**	**1.613**	**1.444**
2θ Angle, °	**29.9**	**34.9**	**35.24**	**36.12**	**42.86**	**57.04**	**64.46**
% Intensity, extracted	79.96	45.76	48.79	100	98.39	30.18	24.74
% Intensity, stripped	62.58	42.31	42.99	66.87	100	25.84	19.11

TABLE 3: Process Changes with corresponding % Conversion		
TOS, hrs	**SA-0946: Change**	**% conversion**
0	Sample; T = 260°C; P = 200 PSIG; H_2/CO = 0.67; SV = 2.34 Nl/g-cat/h	36.1 (2h)
113	Sample	76.6 (112h)
133	SV=1.8 Nl/g-cat/h	76.0 (131h)
229	Sample	80.2 (228h)
231	P = 300 PSIG; SV = 2.64 Nl/g-cat/h	76.4 (235h)
354	Sample	81.1 (351h)
427	Sample	81.0 (426h)
443	H_2/CO = 0.6; SV = 2.0 Nl/g-cat/h	81.5 (442h)
563	Sample	81.9 (561)
TOS, hrs	**SB-3425: Change**	**% Conversion**
0	Sample; H_2/CO = 0.67; T = 260°C; SV = 2.34 Nl/g-cat/h; P = 200 PSIG	75.8 (1.5h)
111	Sample	70.8 (110h)
159	SV = 1.80 Nl/g-cat/h	70.2 (157h)
233	Sample	73.5 (230h)
278.5	Power out	71.8 (276h)
279	T = 200°C	---
282	T = 260°C	70.0 (287h)
311	H2/CO = 0.6	69.8 (310h)
330	Sample	65.1 (329h)
330	SV = 1.0 Nl/g-cat/h	81.7 (340h)
355	T = 266°C	80.0 (353h)
384	Sample	80.1 (383h)

Table 4: Estimated wt % of iron phases in SB-3425, Slurry samples				
TOS, hrs	**α-Fe**	**ϵ′-carbide**	**χ-carbide**	**magnetite**
0	100	0	0	0
111	0.02 (QRSR) 0.03 (I/I_{cor})	99.98 (QRSR) 99.98 (I/I_{cor})	0	0
233	3.09	96.91	0	0
233 (SP1)	*1.76*	*89.50*	---	*8.74*
330	0.42	14.44	85.98	0
384	.004	2.47	97.52	0

SB-3425, Slurry samples: Particle sizes, nm				
TOS, hrs	**α-Fe**	**ϵ′-carbide**	**χ-carbide**	**magnetite**
0	13.54		---	---
111	37.88	5.27	---	---
233	30.50	47.12	---	---
233 (SP1)	17.54	23.32	---	33.42
330	37.88	5.27	7.63	---
384	37.22	4.49	14.78	---

Table 5: Estimated wt % of iron phases in SA-0946, slurry samples				
TOS, hrs	**α-Fe**	**ϵ′-carbide**	**χ-carbide**	**magnetite**
0	0.00	13.41	86.38	0.22
113	0.00	46.17	52.85	0.99
229	0.01	49.46	49.48	1.05
354	0.005	52.92	46.42	0.65
427	0.00	18.25	81.54	0.21
563	0.00	12.19	87.40	0.41

SA-0946, slurry samples: Particle sizes, nm				
TOS, hrs	**α-Fe**	**ϵ′-carbide**	**χ-carbide**	**magnetite**
0	---	13.67	26.92	19.27
113	---	11.38	11.58	48.195
229	52.12	11.27	7.67	44.16
354	7.10	19.44	15.75	189.36
427	---	21.60	21.88	145.86
563	---	29.49	77.34	158.19

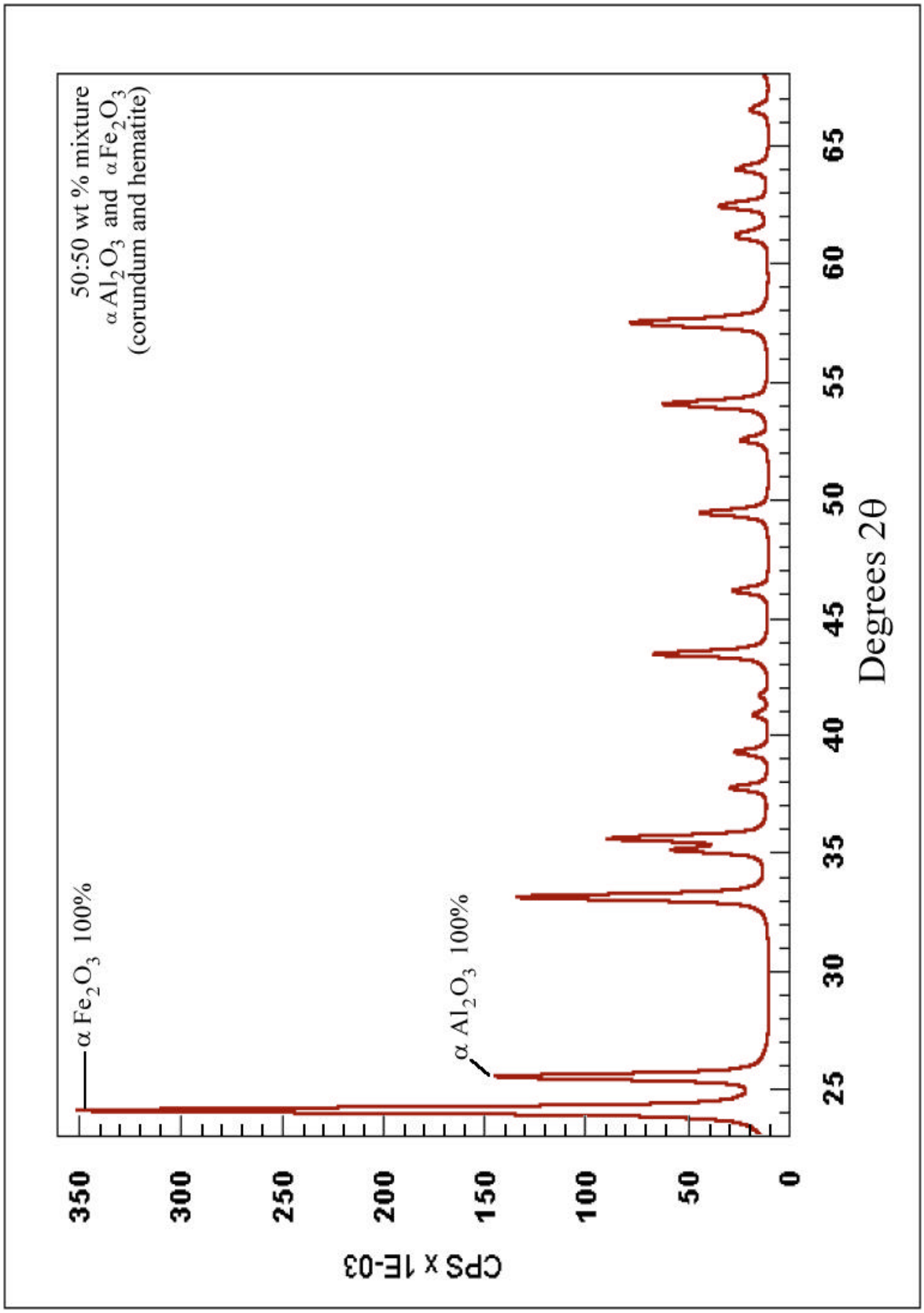

Figure 1 Simulated X-ray diffraction pattern of a 50:50 wt % mixture of hematite (Fe_2O_3) and corundum (α-Al_2O_3). The peak height ratio for the 100% peaks, $I/_{I_{COR}}$, is 2.544.

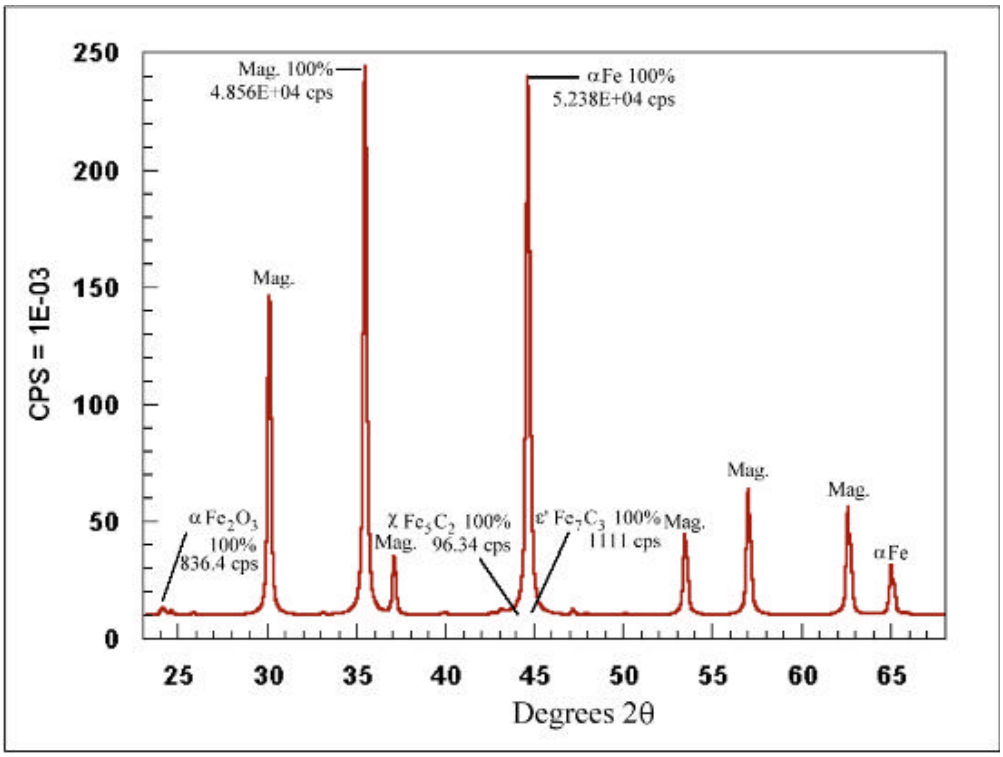

Figure 2a a) Simulated X-ray diffraction pattern for a 20 wt% mixture of each of these phases: Fe_2O_3:Fe_3O_4:α-Fe:Fe_7C_3:Fe_5C_2

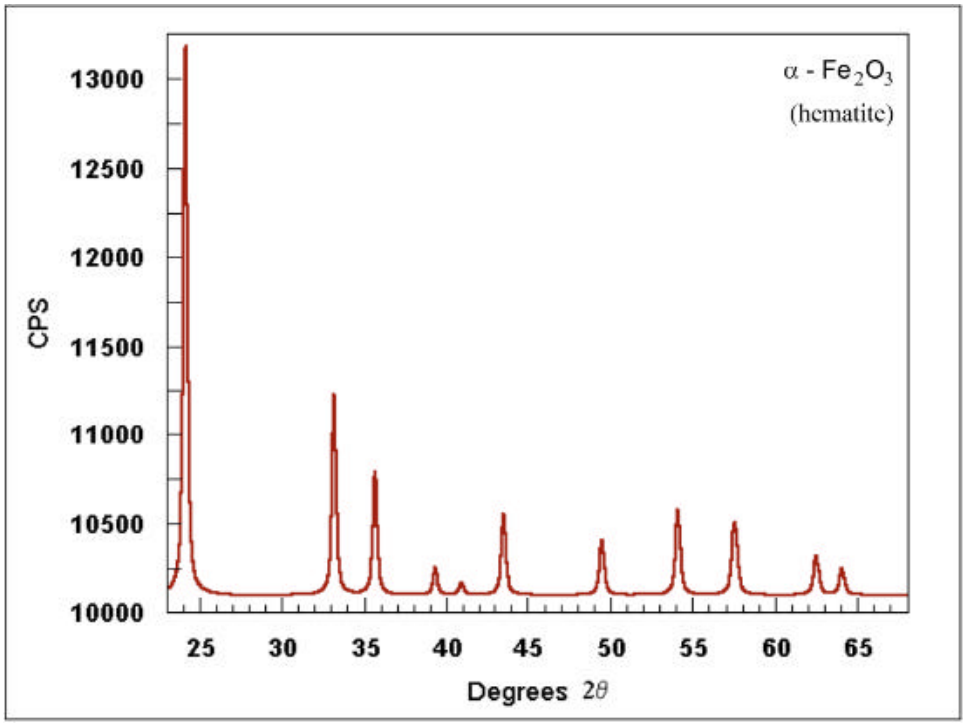

Figure 2b Simulated pattern of Fe_2O_3 from **figure 2a**, plotted at full scale.

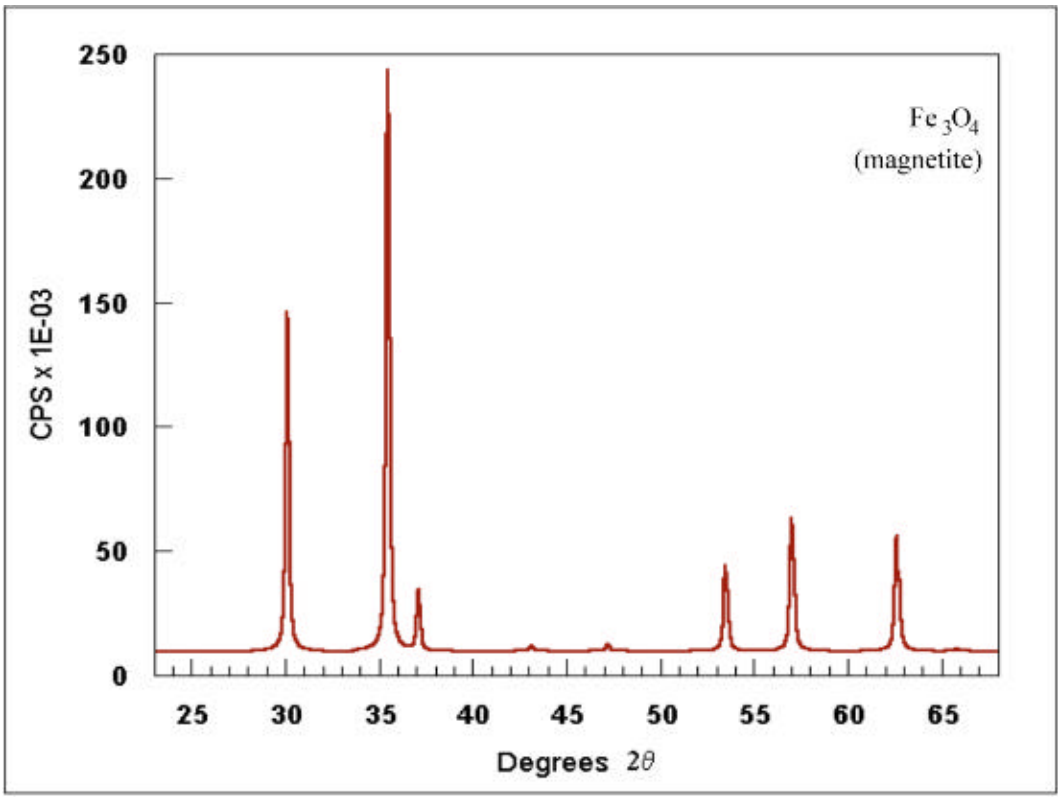

Figure 2c Simulated pattern of Fe_3O_4 from **figure 2a**, plotted at full scale.

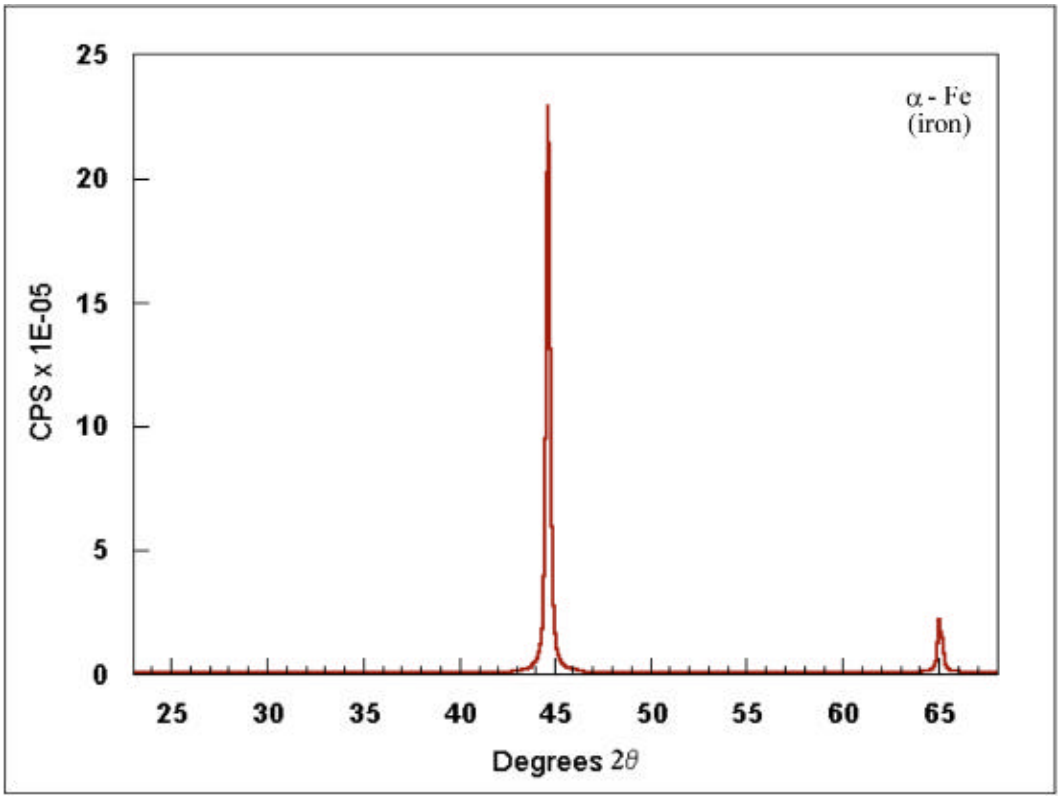

Figure 2d Simulated pattern of α-Fe from **figure 2a**, plotted at full scale.

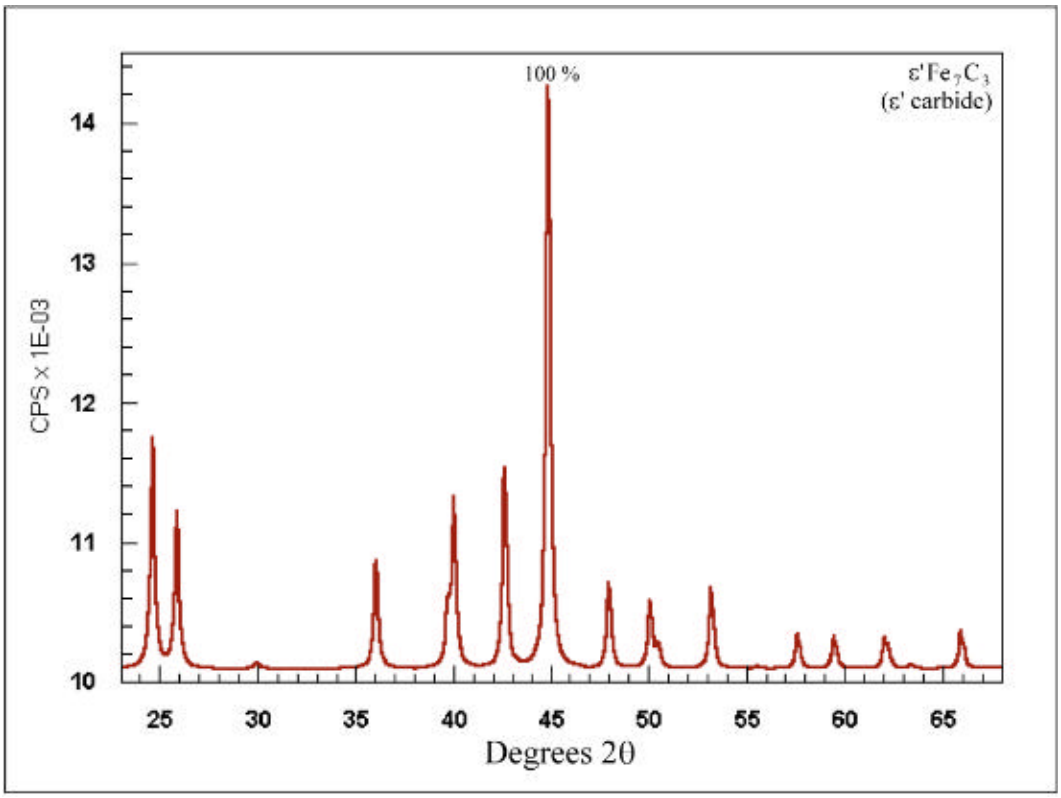

Figure 2e Simulated pattern of Fe_7C_3 from **figure 2a**, plotted at full scale.

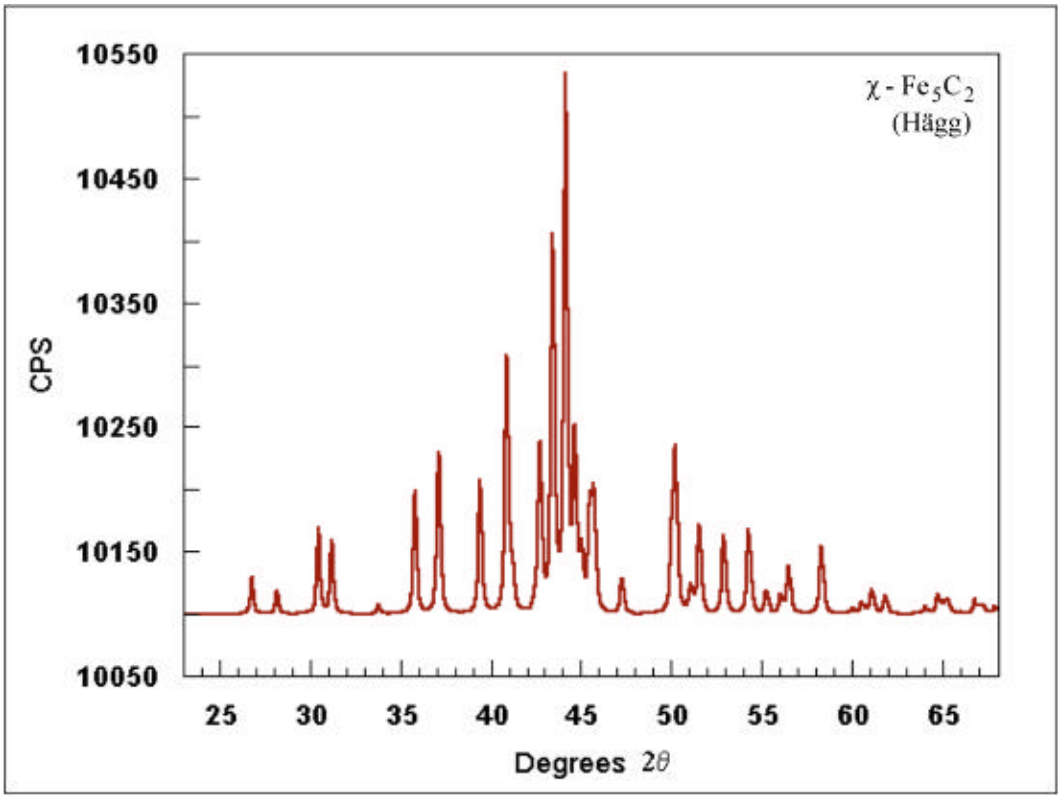

Figure 2f Simulated pattern of Fe_5C_2 from **figure 2a**, plotted at full scale.

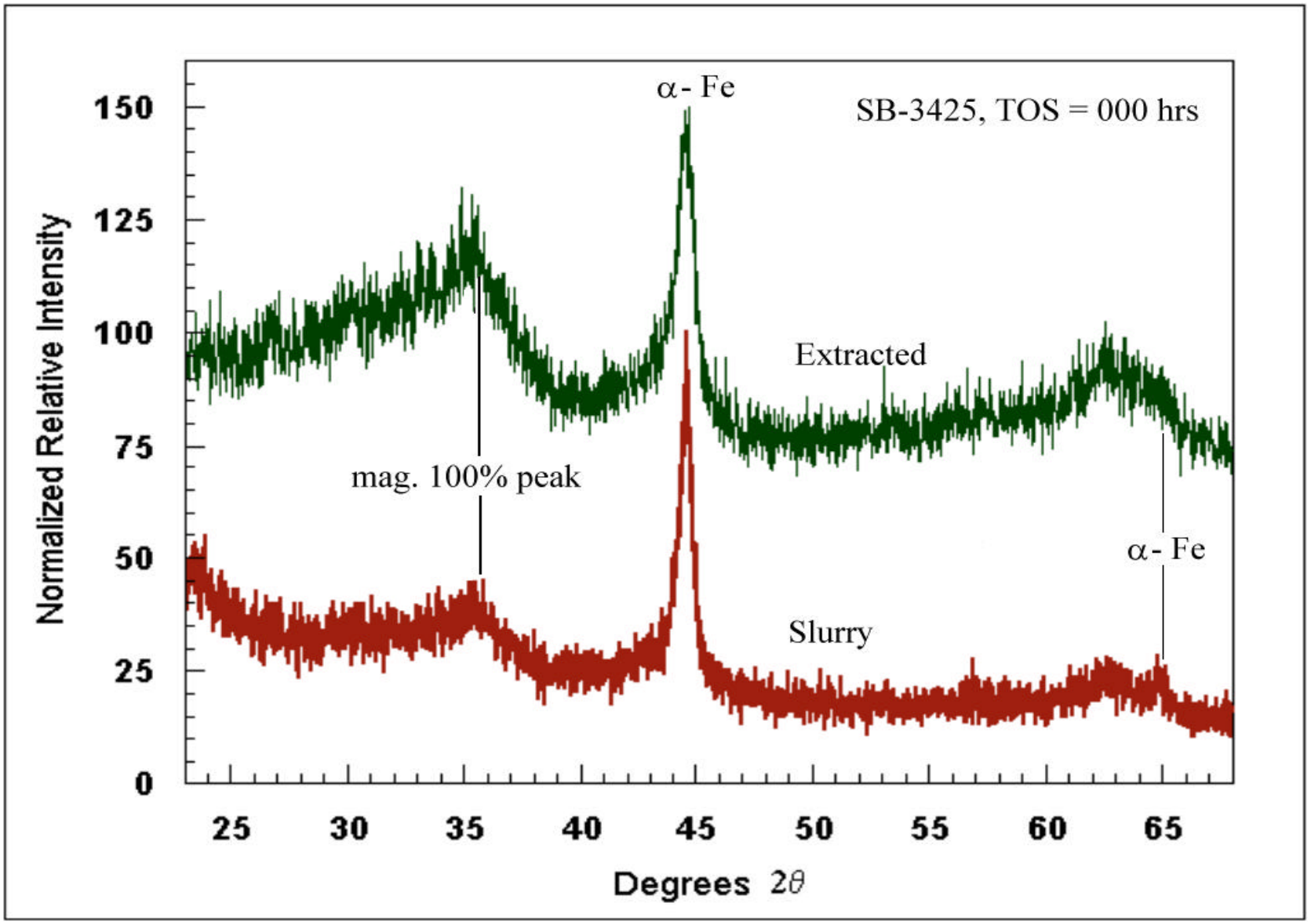

Figure 3 X-ray diffraction pattern from run SB-3425, TOS = 000 hrs. Lower curve, sample in the oil, and upper curve: powder after soxhlet extraction .

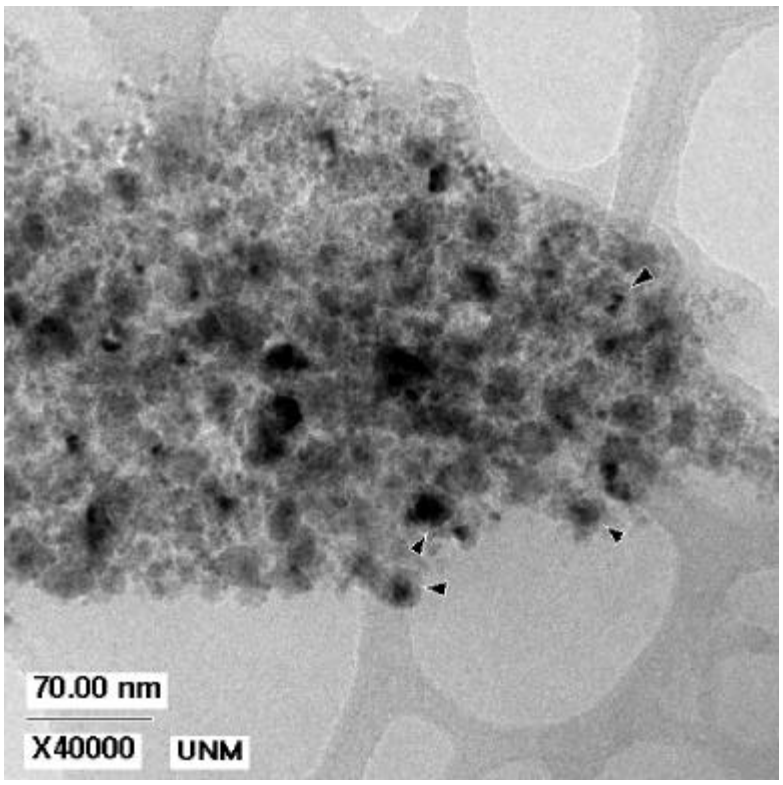

Figure 4a Low magnification view of SB-3425, TOS = 000 hrs, extracted powder

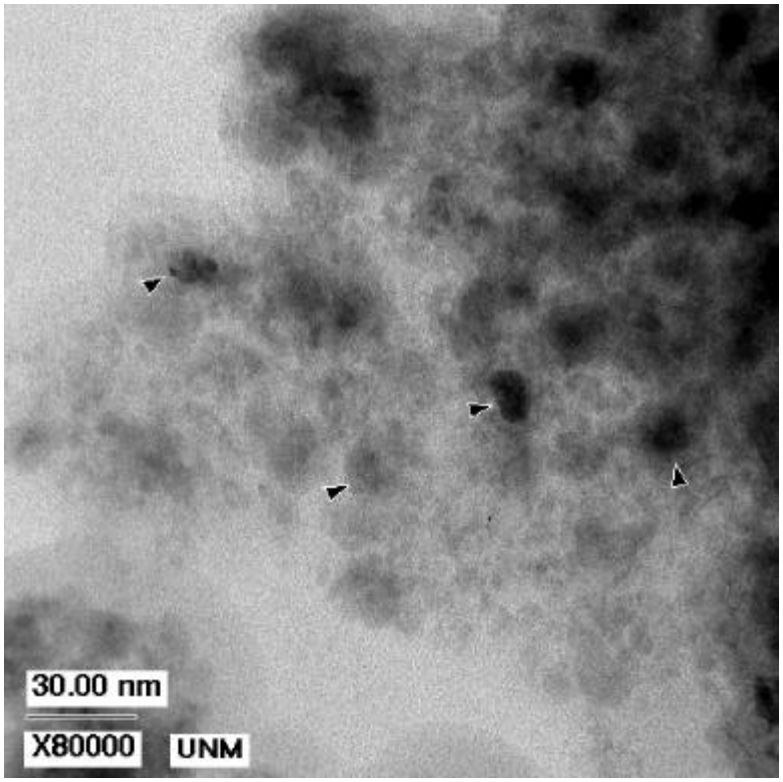

Figure 4b Low magnification view of SB-3425, TOS = 000 hrs, slurry

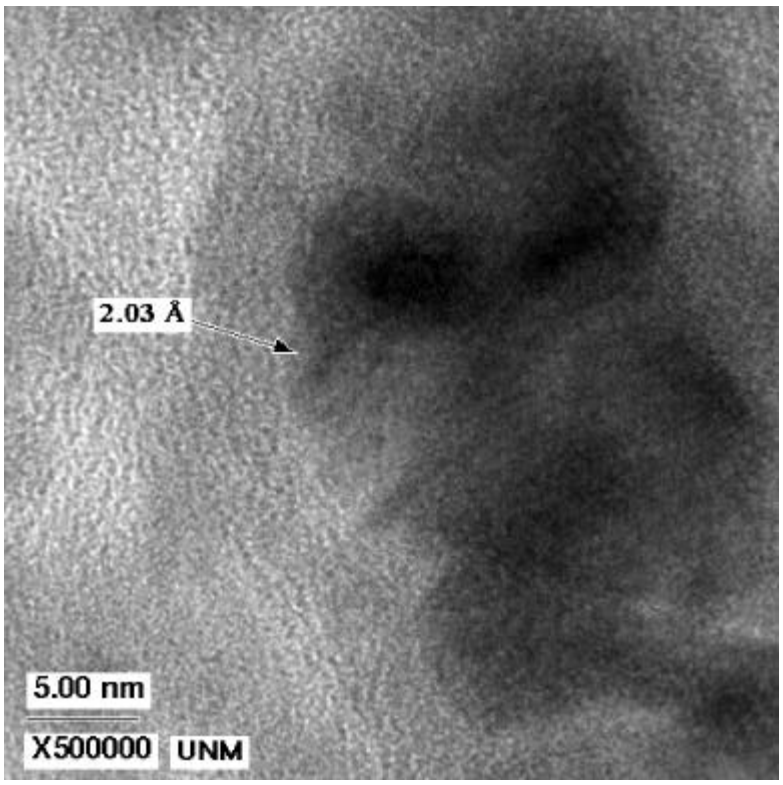

Figure 4c High magnification view of SB-3425, TOS = 000 hrs, extracted powder

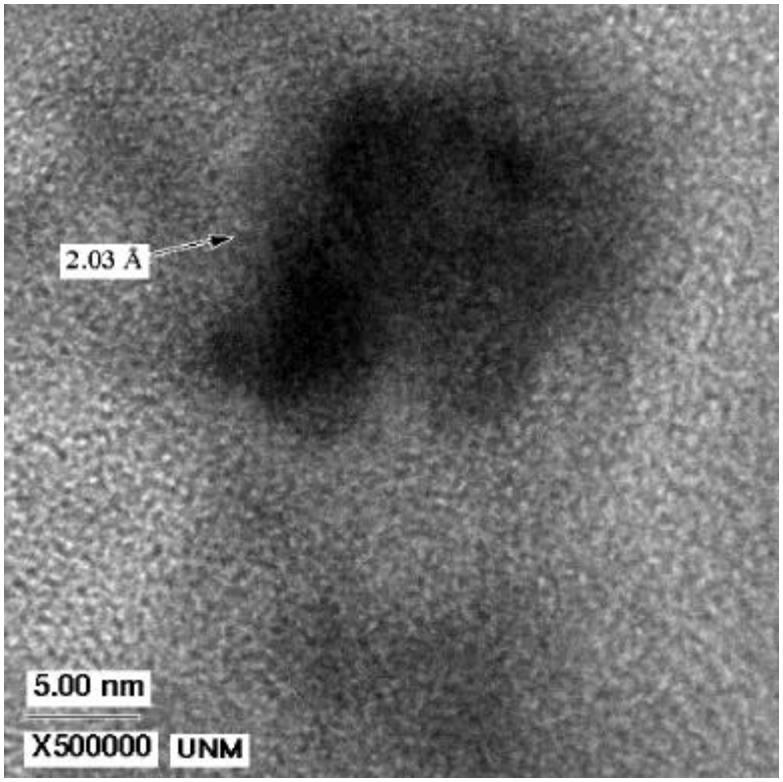

Figure 4d High magnification view of SB-3425, TOS = 000 hrs, slurry

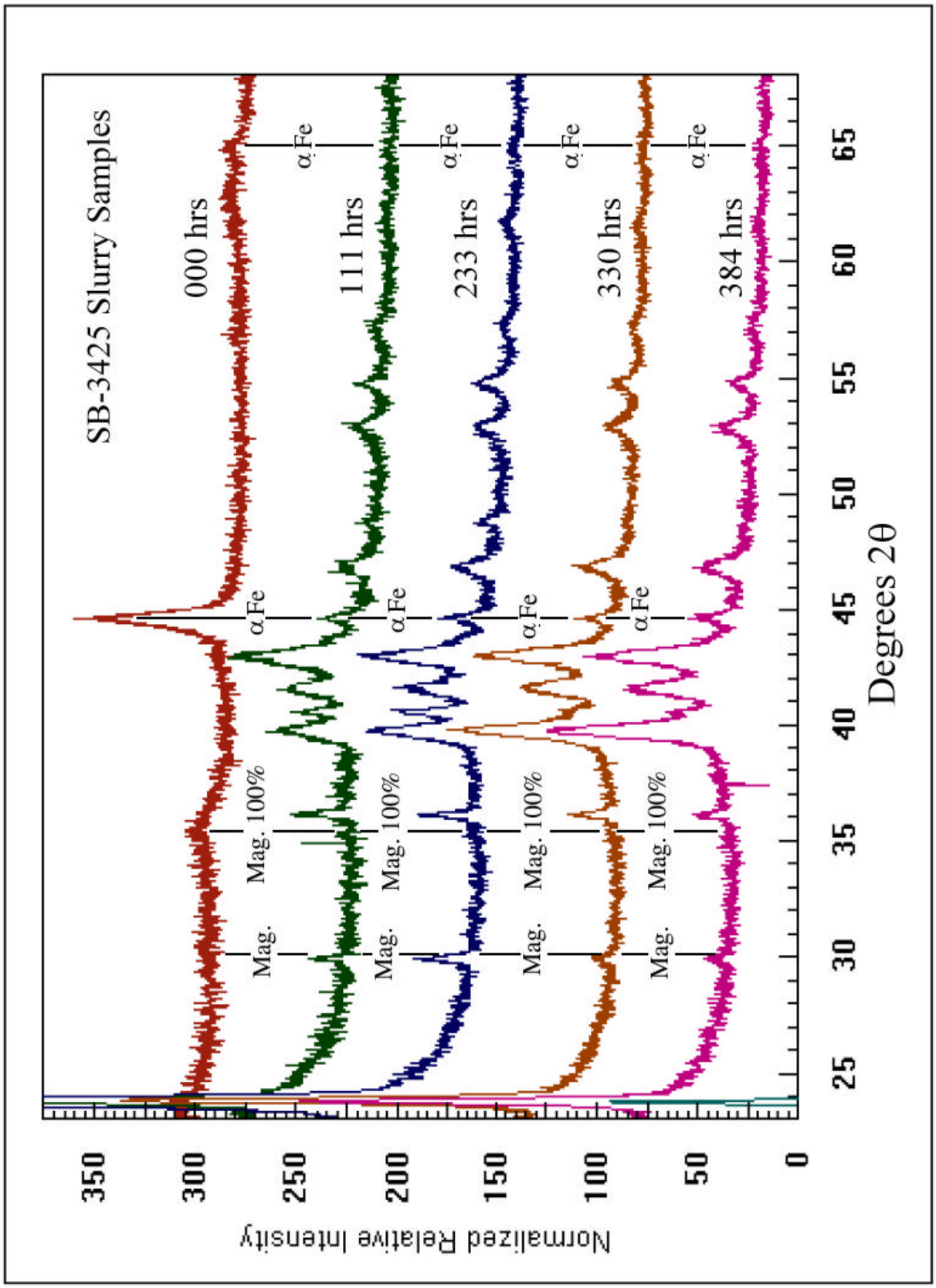

Figure 5a X-ray diffraction of samples from run SB-3425, slurry samples

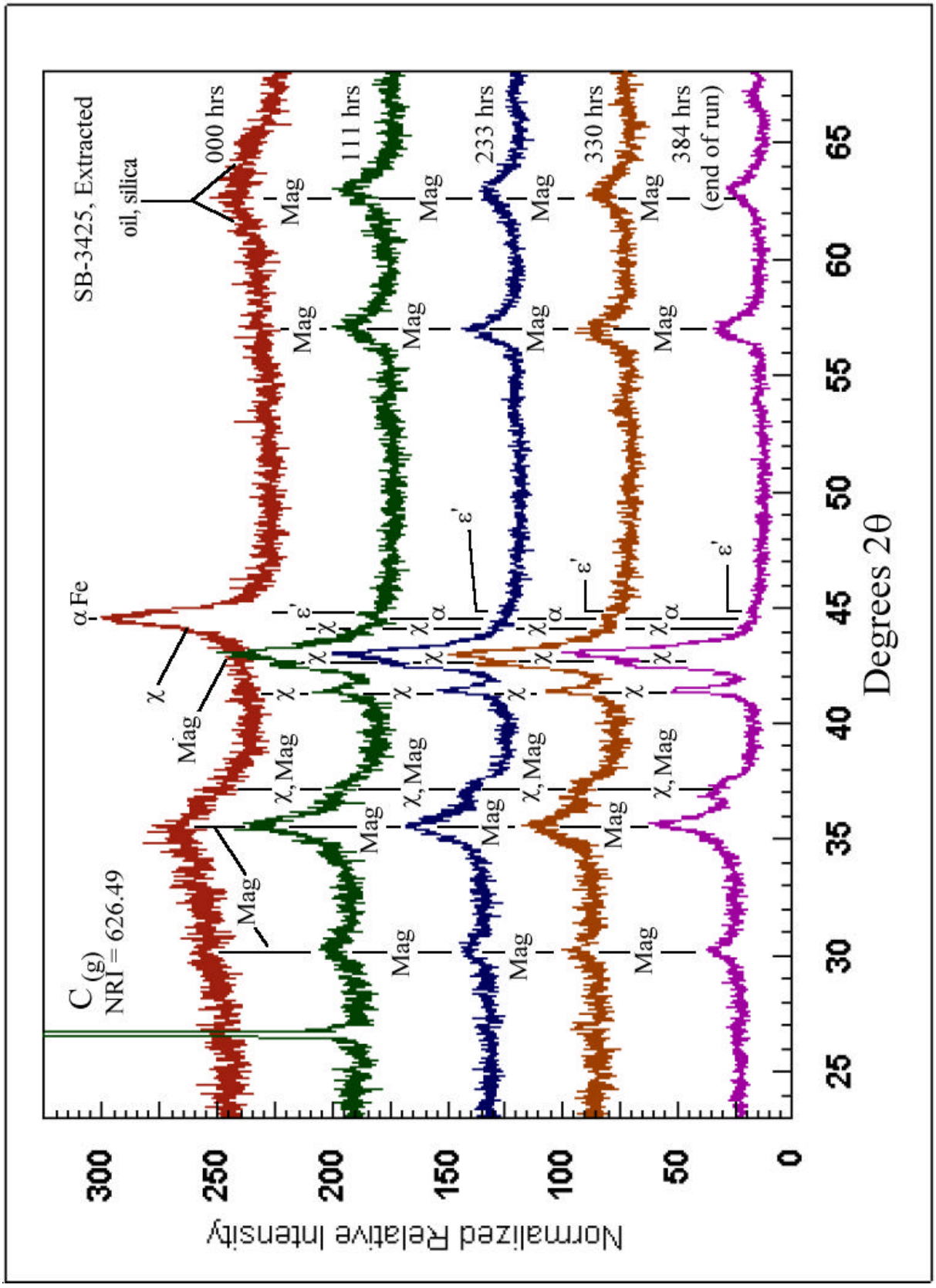

Figure 5b X-ray diffraction of samples from run SB-3425, extracted samples

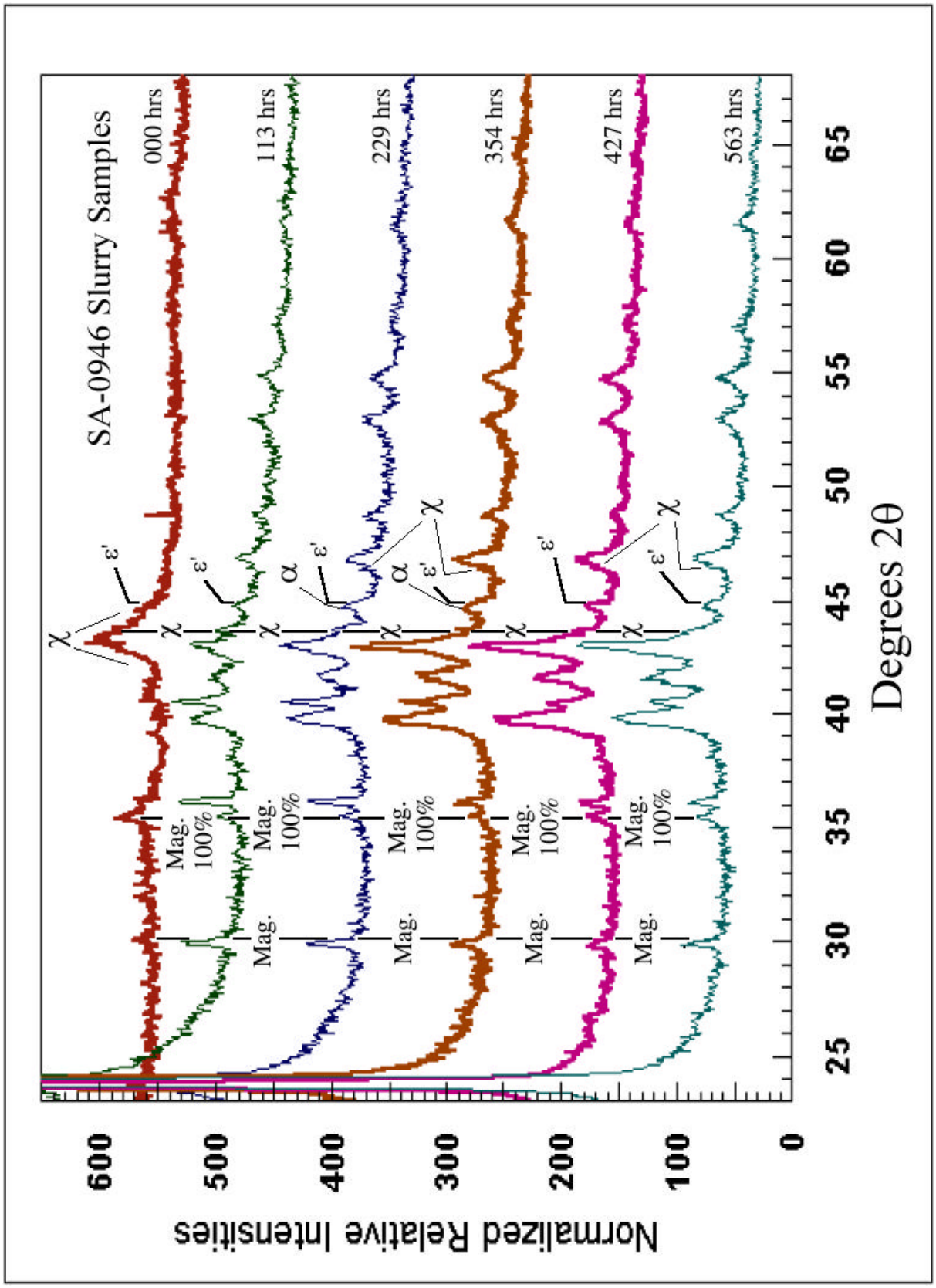

Figure 5c X-ray diffraction of samples from run SA-0946, slurry samples.

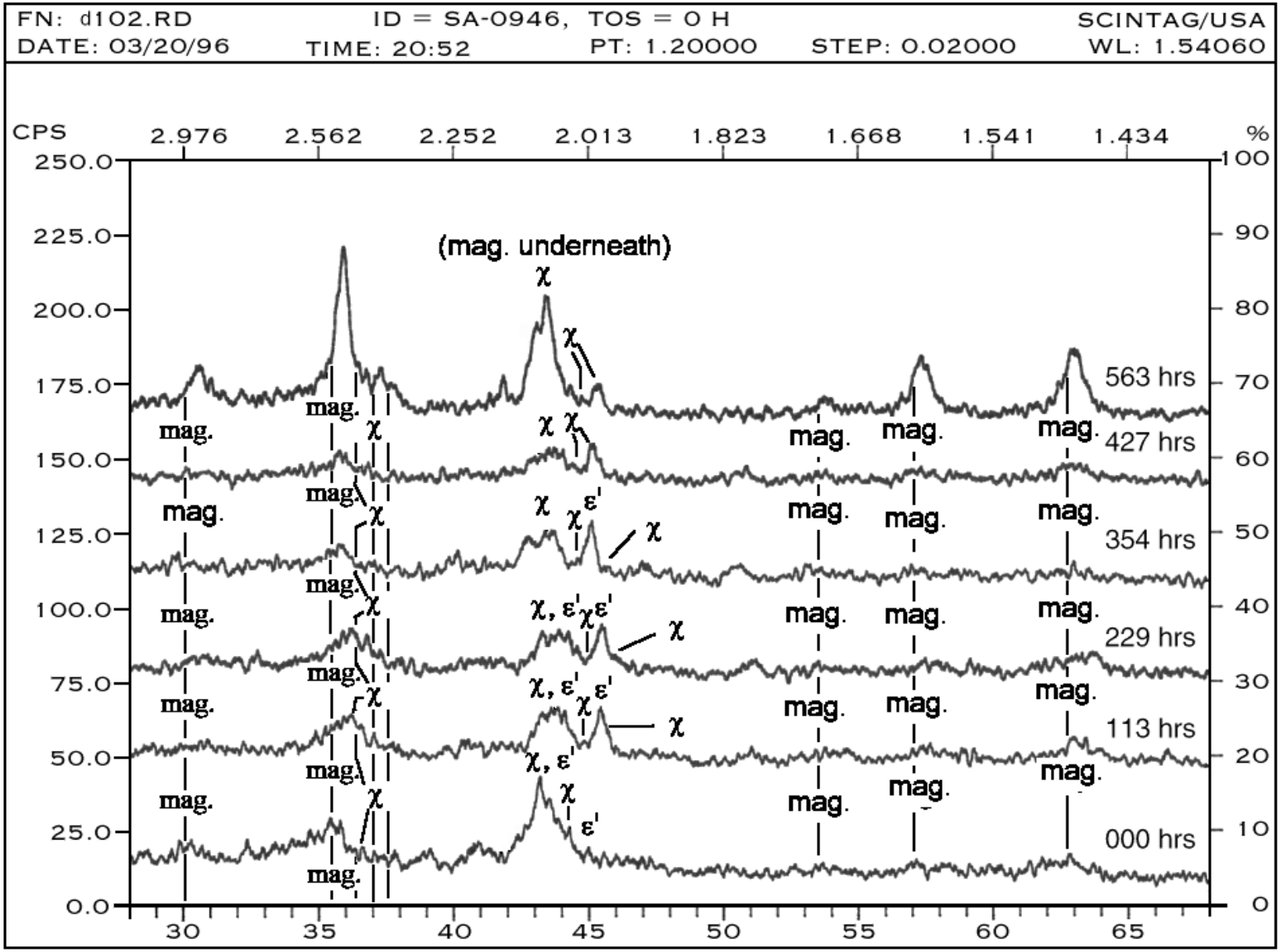

Figure 5d XRD of samples from run SA-0946, extracted.

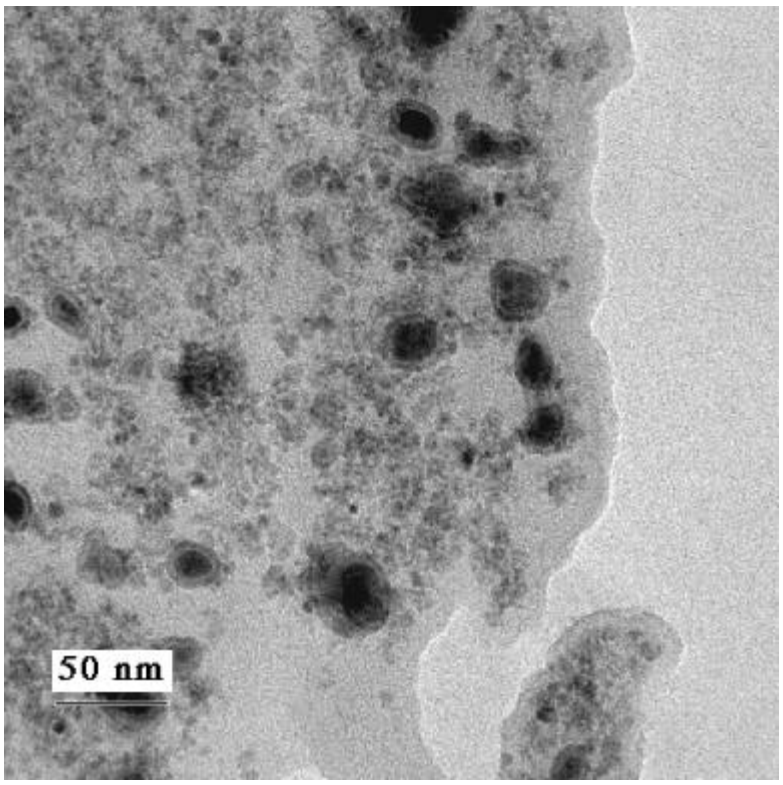

Figure 6a Low magnification view of SB-3425, TOS = 384 hrs, extracted powder.

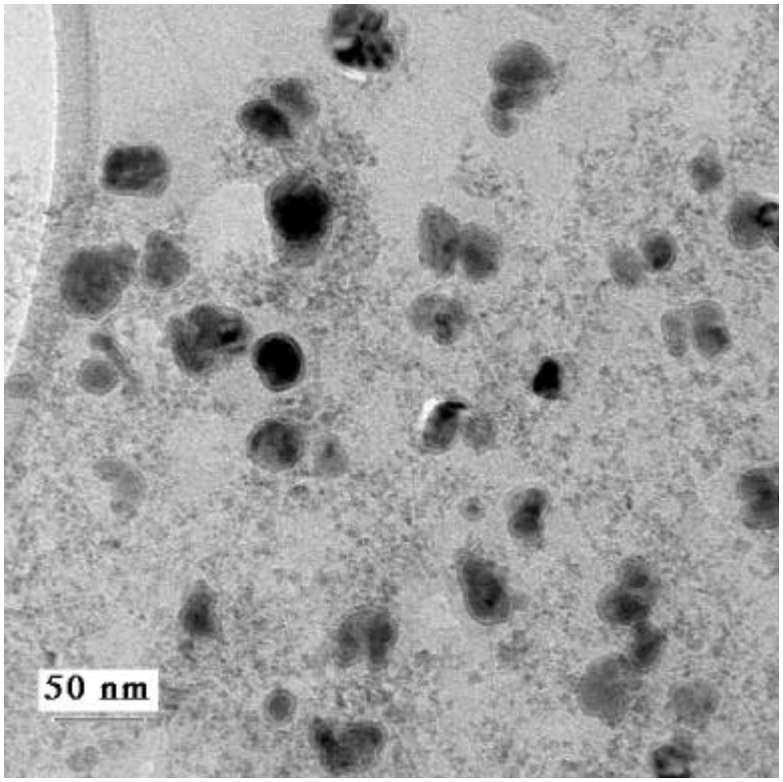

Figure 6b Low magnification view of SB-3425, TOS = 330 hrs, slurry.

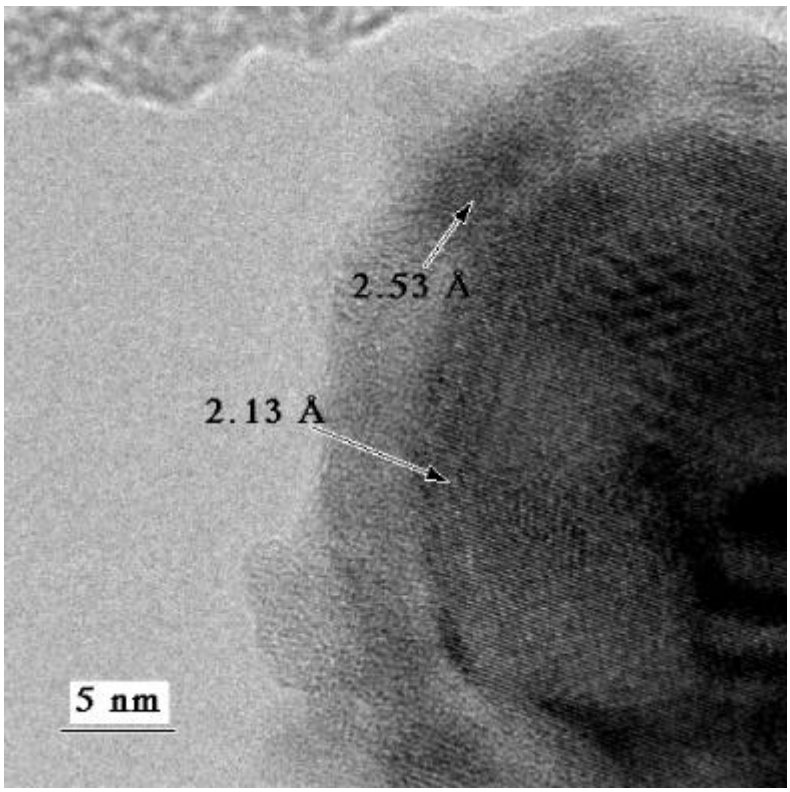

Figure 6c High magnification view of SB-3425, TOS = 384 hrs, extracted powder, no microtomy.

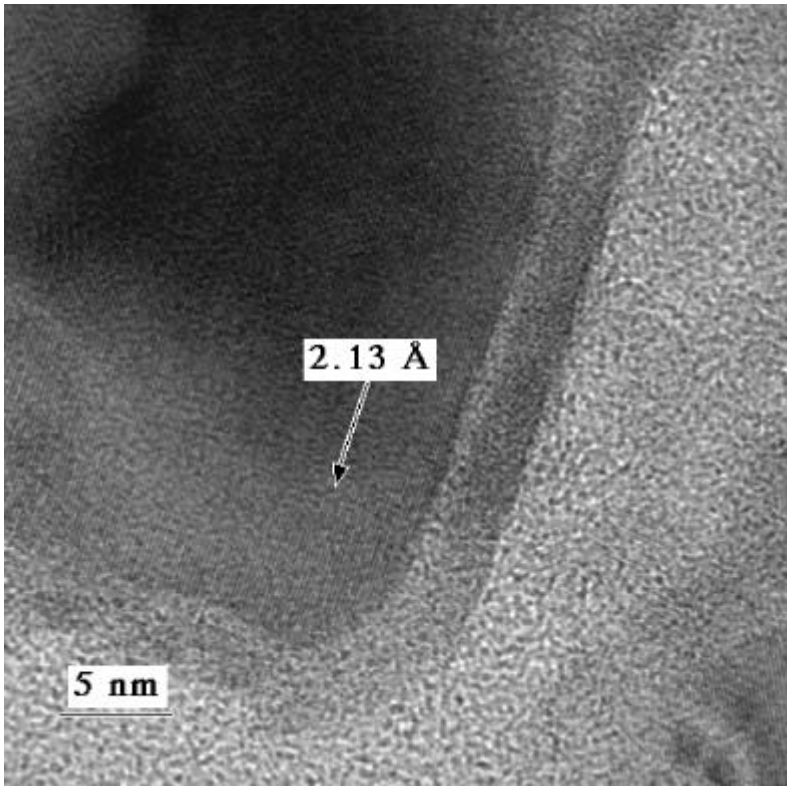

Figure 6d High magnification view of SB-3425, TOS = 330 hrs, slurry.

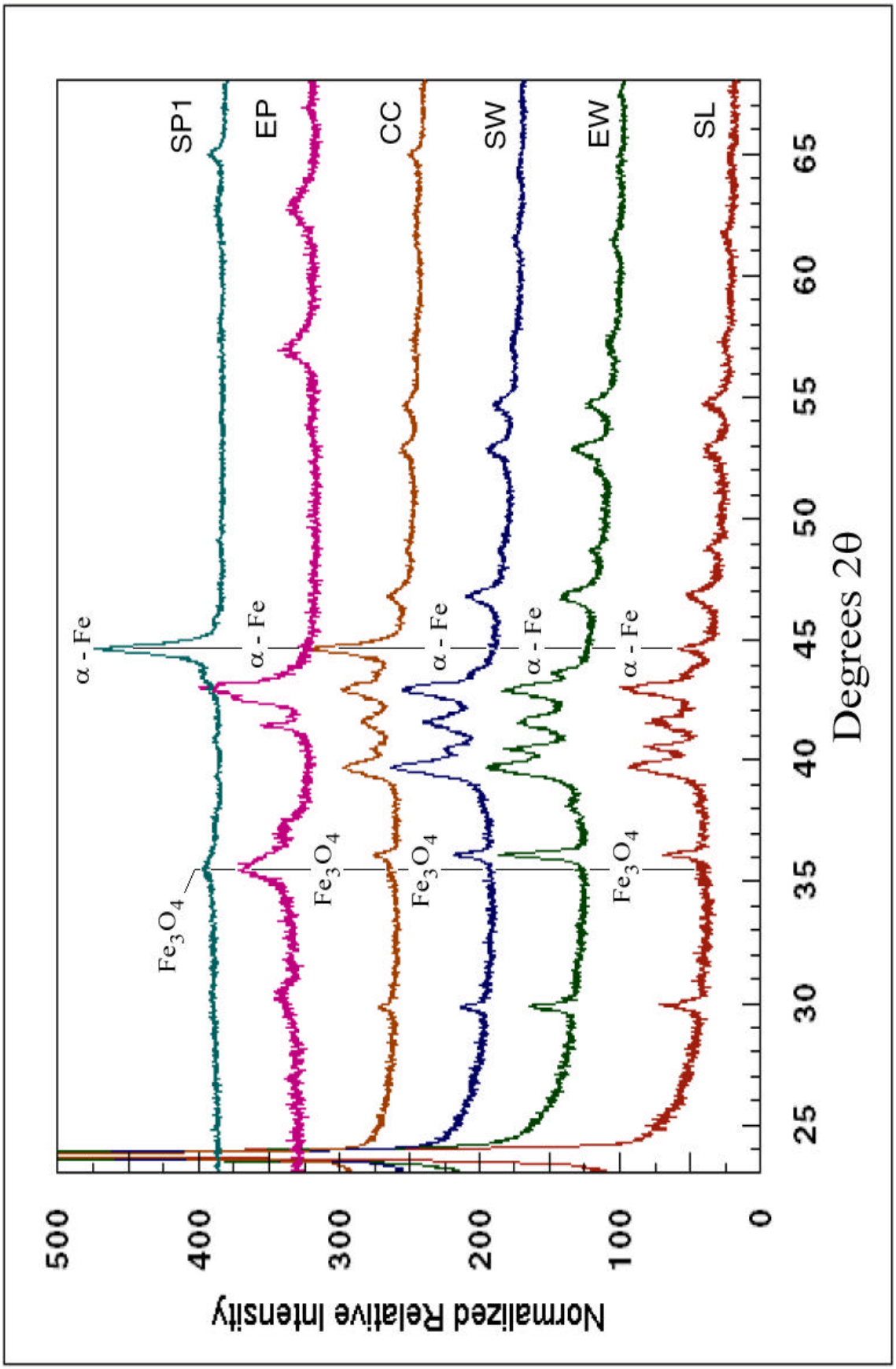

Figure 7 XRD patterns of samples from SB-3425, TOS = 233 hrs. Original slurry (SL), soxhlet-extracted wax (EW), inert-stripped wax (SW), catalyst concentrated by sedimentation (CC), soxhlet-extracted powder (EP), and inert-stripped powder (SP).

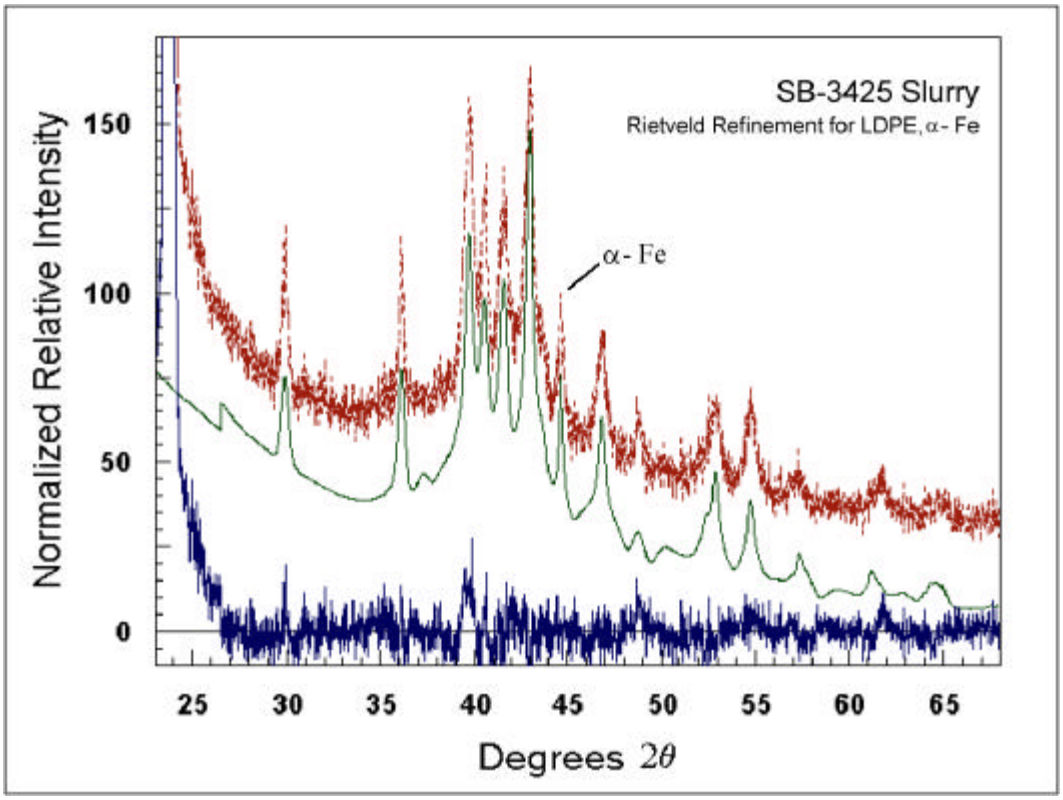

Figure 8a Incomplete Rietveld refinement of SB-3425, TOS = 233 hrs, for wax (LDPE structure) and α-Fe.

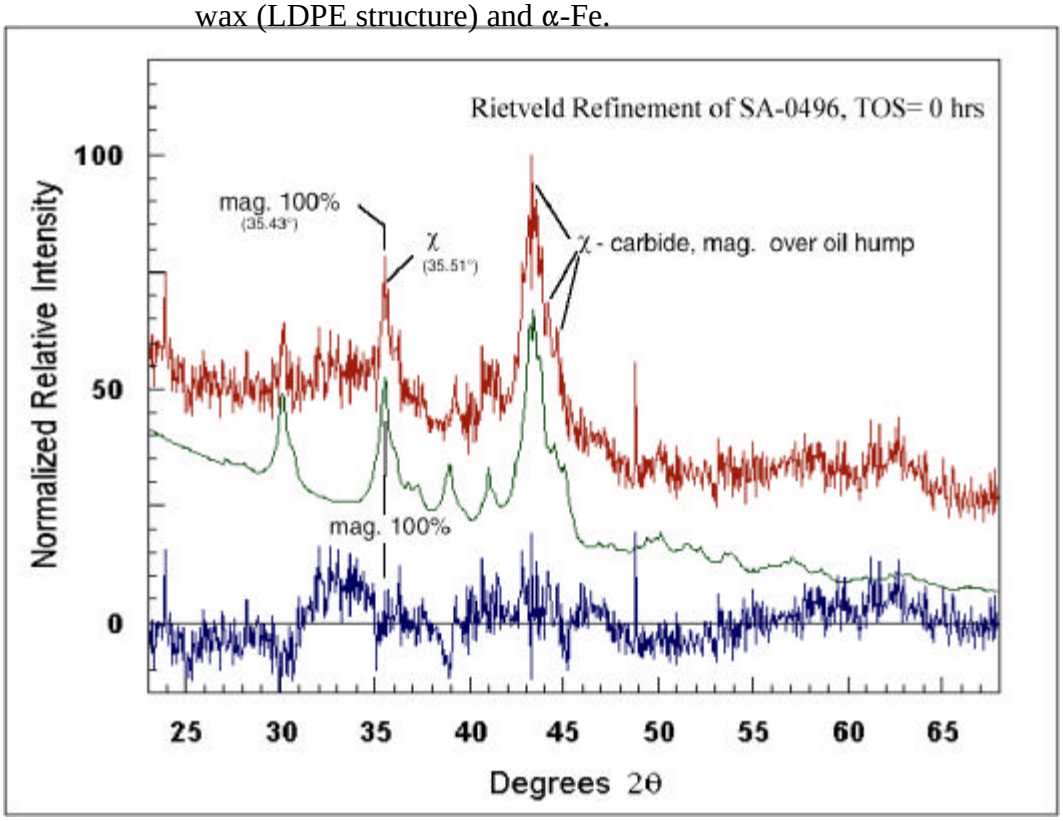

Figure 8b Rietveld refinement of SA-0946, TOS = 000 hrs, catalyst in oil, for magnetite, χ-carbide, and ϵ′-carbide.

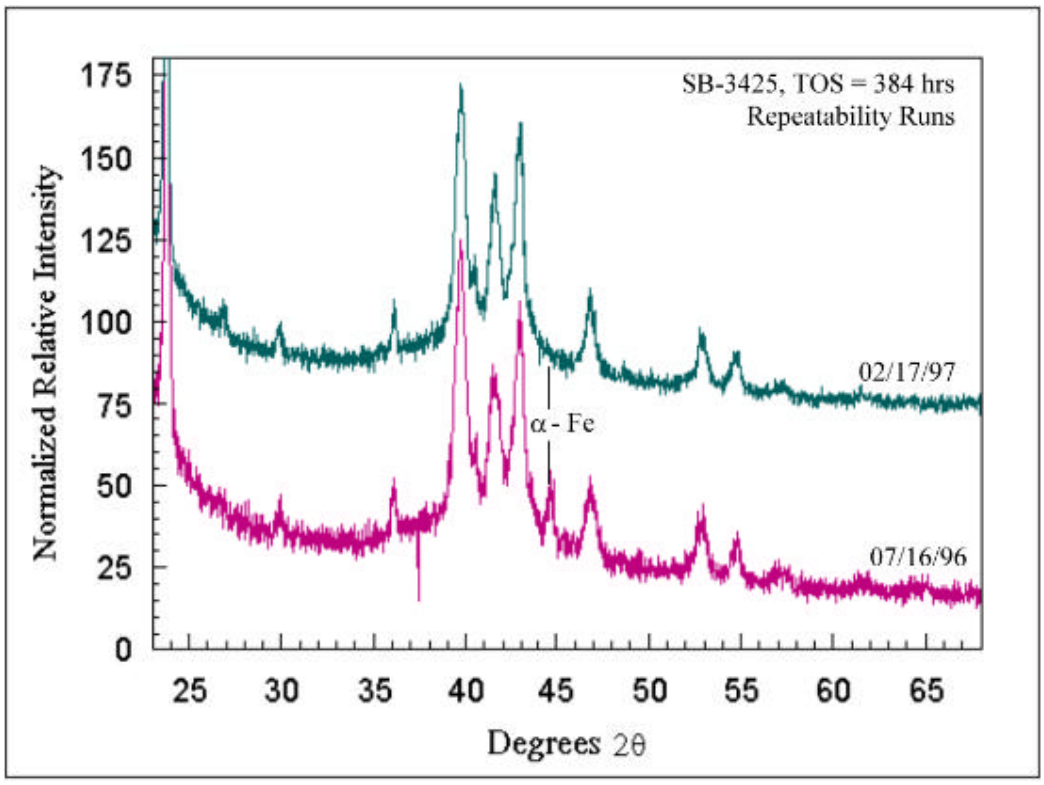

Figure 9a XRD plot of SB-3425, TOS = 384 hrs, slurry, and repeat analysis after 7 months.

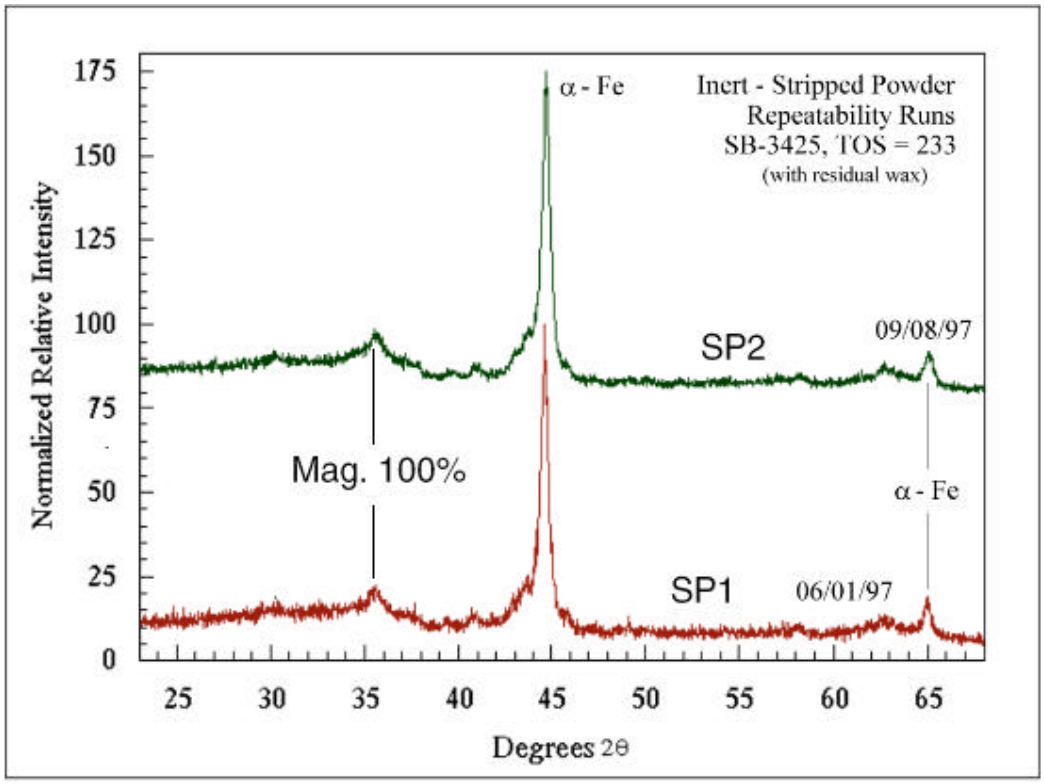

Figure 9b XRD plot of SB-3425, TOS = 233, stripped powder after 1 month, with repeat analysis after 3 months.

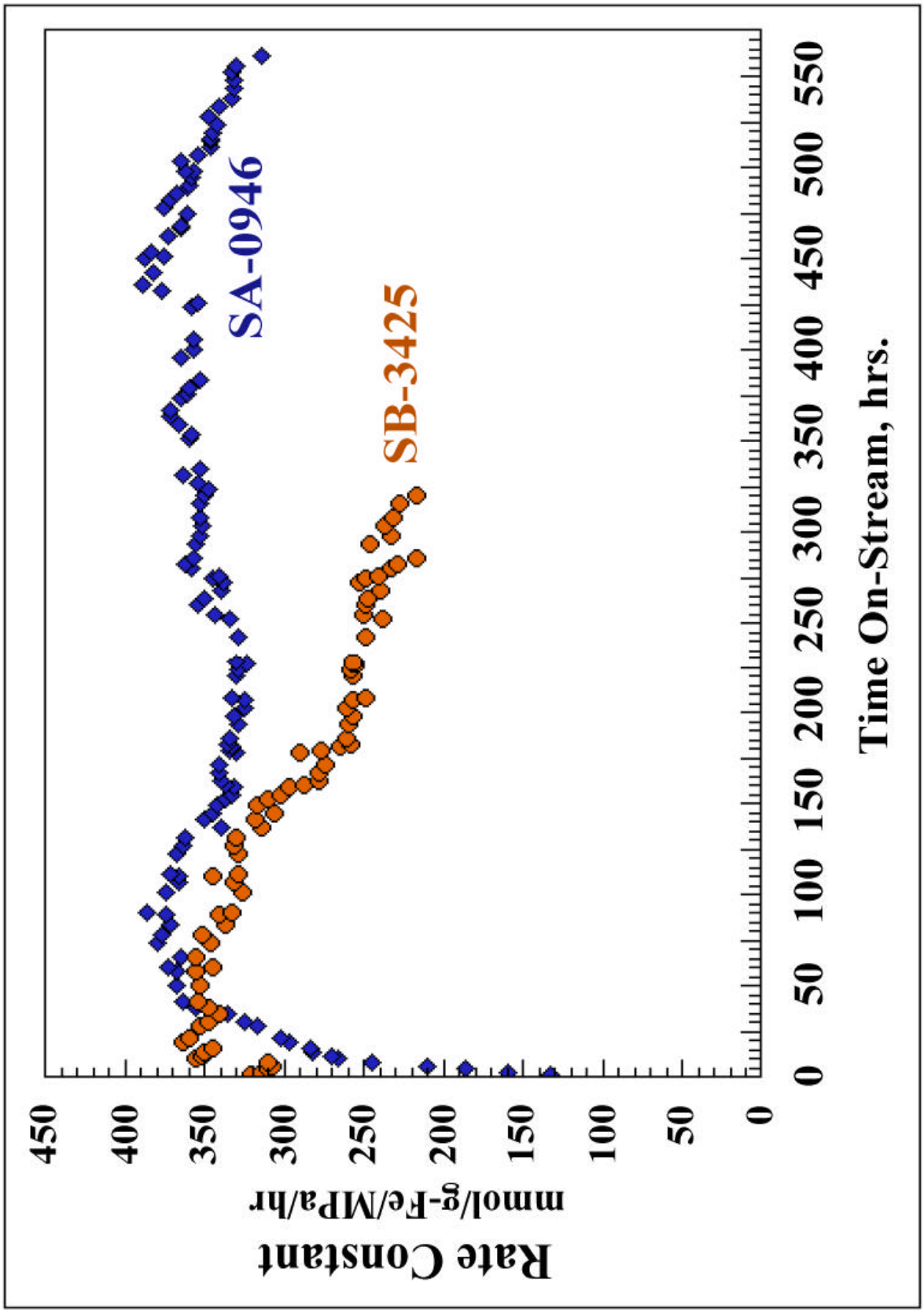

Figure 10 Fischer-Tropsch reactivity curves for runs SB-3425, and SA-0946, plotted as a pseudo first order rate constant referenced to 260°C, in mmol of CO converted per g Fe per MPa pressure per hour. (Ref. Table 3).